



FROM DISEASE GENE IDENTIFICATION TO THERAPEUTIC TARGETS  
IN NEUROMUSCULAR DISEASES

A dissertation submitted in partial satisfaction of the requirements for the degree

Doctor of Philosophy in Neuroscience

by

Carlo Rinaldi, M.D

Doctoral School of Molecular Medicine  
Department of Neuroscience,  
Reproductive and Odontostomatological Sciences  
University of Federico II  
Via Sergio Pansini  
80121, Napoli  
Italia

Neurogenetics Branch, NINDS, NIH  
Porter Neuroscience Research Center  
Building 35, Room 2A-1000  
35 Convent Drive, MSC 3705  
Bethesda, MD 20892-3705  
USA

Supervisors:

Prof. Giuseppe De Michele

Prof. Kenneth H. Fischbeck

February 2014

## Table of Contents

Title Page.....	1
Acknowledgements and Dedication.....	2
Introduction.....	6
References.....	8
 Chapter 1. Cowchock Syndrome (CMTX4) is Associated with Apoptosis-Inducing Factor (AIFM1) Mutation:	
Introduction.....	12
Materials and Methods.....	12
Results.....	14
Acknowledgments.....	23
Web Resources.....	24
References.....	25
Figure Legends.....	30
Figures.....	34
Table.....	38
Supplemental Data.....	40
 Chapter 2-1. Spinal and bulbar muscular atrophy: from disease pathogenesis to clinical management:	
Introduction.....	46
From AR functions to motorneuron disease: pathophysiology of SBMA...	47

Diagnostic studies and evaluation.....	50
Clinical Presentation.....	52
Differential Diagnosis.....	54
Management.....	55
References.....	57
Figure Legends.....	64
Figures.....	65

Chapter 2-2. Case Report: Early onset and novel features in a spinal-bulbar muscular atrophy patient with a 68 CAG repeat:

Case.....	68
Discussion.....	69
References.....	71
Figure Legends.....	72
Figures.....	73

Chapter 2-3. IGF-1 ameliorates disease manifestations in a mouse model of SBMA:

Introduction.....	75
Materials and Methods.....	75
Results.....	78
Discussion.....	80
Acknowledgments.....	81
References.....	82

Figure Legends.....	86
Figures.....	89
Supplemental Data.....	92

## **ACKNOWLEDGEMENTS AND DEDICATION**

Quello che segue é il frutto di anni di sacrifici e lavoro intenso: lunghi giorni al microscopio, innumerevoli fine settimana ad analizzare dati, e poi un continente nuovo, una lingua diversa, un lavoro mai fatto prima, il dover affrontare tutto per la prima volta.

Non ci sarei riuscito senza il supporto di tutte le persone che ho incontrato sulla strada, primo tra tutti il mio mentore, Kurt Fischbeck, i membri passati e presenti del laboratorio, gli scienziati con cui ho scambiato appassionate conversazioni e gli amici di tutto il mondo che adesso sono come famiglia per me.

Ringrazio i miei tutor nei miei altrettanto importanti anni di clinica, prof. Giuseppe De Michele e prof. Alessandro Filla: da voi ho imparato la Neurologia, il rigore scientifico e l'onestá intellettuale. Vi devo molto.

Grazie alla mia famiglia che amo profondamente: siete la mia sicurezza.

E soprattutto grazie a mia moglie per essere sempre al mio fianco e al mio piccolo figlio, sei la mia felicità.

## **INTRODUCTION**

Neuromuscular diseases include a wide range of acquired or inherited conditions mainly affecting the motor neurons in the spinal cord, peripheral motor nerves, and/or the muscles.

The overall estimated prevalence of the various inherited neuromuscular diseases (including the most common forms of muscular dystrophy, proximal spinal muscular atrophies, and the hereditary motor and sensory neuropathies) among both sexes is approximately 1 in 3500 in the general population, according to a meta-analysis of over 150 published studies (Emery AE, 1991).

Although medical interventions have increased the life span and improved the quality of life for many of these diseases, at present there is still no cure for most neuromuscular diseases, and many familiar cases still remains with no genetic diagnosis.

The recent advances in genetics together with the widespread availability of whole genome and exome sequencing has effectively removed many obstacles in the process of disease gene identification, like the need of large pedigrees.

Disease gene identification allows to the development of cell culture and animal models for delineating disease mechanisms, and it facilitates the identification of targets for therapeutic intervention.

The overall purpose of my PhD research is to investigate the causes of hereditary neurological diseases, with the goal of developing effective treatments for these

disorders. This purpose is pursued through two strategic aims: (1) To identify and characterize novel disease genes for hereditary neuromuscular and neurodegenerative disorders. (2) To develop and evaluate potential therapeutic agents for spinal and bulbar muscular atrophy (SBMA).

Specific aim 1. To identify and characterize novel disease genes for hereditary neuromuscular and neurodegenerative disorders

Charcot-Marie-Tooth disease (CMT) defines a clinically and genetically heterogeneous group of hereditary peripheral neuropathies characterized by chronic motor and sensory impairment. Charcot-Marie-Tooth disease is the most common hereditary neuromuscular disorder, with a prevalence of ~1 in 2,500 people (Skre, 1974). Approximately 7-10% of CMT is inherited as an X-linked trait (CMTX) (Pareyson, 2009). We have evaluated a large Italian-American family with a slowly progressive, childhood-onset, X-linked recessive axonal neuropathy with deafness and cognitive impairment. By using the means of next generation sequences, we have found that mutation in *AIFM1* causes this form of CMTX.

Specific aim 2. To develop and evaluate potential therapeutic agents for spinal and bulbar muscular atrophy (SBMA).

Spinal and bulbar muscular atrophy (SBMA) is an inherited motor neuron disease caused by a trinucleotide (CAG) repeat expansion in the androgen receptor (AR) gene on the X chromosome (La Spada *et al*, 1991).

To accomplish Specific aim 2, I have used a transgenic mouse model carrying the full-length human AR containing 97 CAGs, gift of Dr. Sobue. These mice demonstrated progressive motor impairment and neuropathologic changes equivalent to human SBMA and are an established model of the disease (Katsuno, 2002). We have investigated the efficacy of treatment with recombinant human IGF-1 in complex with IGFBP-3 (Iplex, mecasemin rinfabate), based on strong in vitro evidence that IGF-1 reduces toxicity of the expanded polyglutamine AR, in a manner dependent upon phospho-inositol-3-kinase (Palazzolo, 2007).

## References

1. Emery AE. (1991). Population frequencies of inherited neuromuscular diseases-a world survey. *Neuromuscula Disord.* 1, 19-29.
2. Skre, H. (1974). Genetic and clinical aspects of Charcot-Marie-Tooth's disease. *Clin. Genet.* 6, 98-118.
3. Pareyson, D., Marchesi, C. (2009). Diagnosis, natural history, and management of Charcot-Marie-Tooth disease. *Lancet Neurol.* 8, 654-667.

4. La Spada AR, Wilson EM, Lubahn DB, Harding AE, Fischbeck KH (1991). Androgen receptor gene mutations in X-linked spinal and bulbar muscular atrophy. *Nature* 352: 77-79.
5. Katsuno, M., Adachi, H., Kume, A., Li, M., Nakagomi, Y., Niwa, H., Sang, C., Kobayashi, Y., Doyu, M., and Sobue, G. (2002). Testosterone reduction prevents phenotypic expression in a transgenic mouse model of spinal and bulbar muscular atrophy. *Neuron* 35: 843–854.
6. Palazzolo I, Burnett BG, Young JE, et al. Akt blocks ligand binding and protects against expanded polyglutamine androgen receptor toxicity. *Hum Mol Genet* 2007;16:1593–1603.

## **Chapter 1**

### **Cowchock Syndrome (CMTX4) is Associated with Apoptosis-Inducing Factor (*AIFM1*) Mutation**

**Carlo Rinaldi,<sup>1</sup> Christopher Grunseich,<sup>1</sup> Irina F. Sevrioukova,<sup>2</sup> Alice Schindler,<sup>1</sup> Iren Horkayne-Szakaly,<sup>3</sup> Costanza Lamperti,<sup>4</sup> Guida Landouré,<sup>1,5</sup> Marina L. Kennerson,<sup>6</sup> <sup>7</sup> Barrington G. Burnett,<sup>1</sup> Carsten Bönnemann,<sup>1</sup> Leslie G. Biesecker for the NIH Intramural Sequencing Center,<sup>8</sup> Daniele Ghezzi,<sup>4</sup> Massimo Zeviani<sup>4</sup> & Kenneth H. Fischbeck<sup>1</sup>**

<sup>1</sup>Neurogenetics Branch, National Institute of Neurological Disorders and Stroke, National Institutes of Health, Bethesda, MD, 20892-3705, USA

<sup>2</sup>Department of Molecular Biology and Biochemistry, University of California, Irvine, CA, 92697-3900, USA

<sup>3</sup>Joint Pathology Center Neuropathology & Ophthalmic Pathology, Silver Spring, MD, 20910-1290, USA

<sup>4</sup>Division of Molecular Neurogenetics, The “Carlo Besta” Neurological Institute Foundation, Istituto di Ricovero e Cura a Carattere Scientifico, Milan, 20126, Italy

<sup>5</sup>Service de Neurologie, Centre Hospitalier Universitaire du Point "G", Bamako, BP  
1805, Mali

<sup>6</sup>Northcott Neuroscience Laboratory, ANZAC Research Institute, University of  
Sydney, Concord, NSW 2139, Australia

<sup>7</sup>Molecular Medicine Laboratory, Concord Hospital, Concord, NSW 2139, Australia

<sup>8</sup>Genetic Disease Research Branch, and NIH Intramural Sequencing Center, National  
Human Genome Research Institute, National Institutes of Health, Bethesda, MD,  
20892-3705, USA

## Introduction

Cowchock syndrome (CMTX4) is a slowly progressive X-linked recessive disorder with axonal neuropathy, deafness, and cognitive impairment. The disease locus was previously mapped to an 11 cM region at chromosome Xq24-q26. Exome sequencing of a patient from the originally described family identified a missense change c.1478A>T (p.Glu493Val) in *AIFM1*, the gene encoding apoptosis-inducing factor (AIF) mitochondrion-associated 1. The change is at a highly conserved residue and co-segregated with the phenotype in the family. AIF is an FAD-dependent NADH oxidase that is imported into mitochondria. With apoptotic insults, a N-terminal transmembrane linker is cleaved off, producing a soluble fragment that is released into the cytosol and then transported into the nucleus, where it triggers caspase-independent apoptosis. Another *AIFM1* mutation that predicts p.Arg201del has recently been associated with severe mitochondrial encephalomyopathy in two infant patients by impairing oxidative phosphorylation. The c.1478A>T (p.Glu493Val) mutation found in the family reported here alters the redox properties of the AIF protein and results in increased cell death via apoptosis, without affecting the activity of the respiratory chain complexes. Our findings expand the spectrum of AIF-related disease and provide new insights into the effects of *AIFM1* mutations.

## Materials and Methods

**Exome data analysis.** Libraries were prepared using NimbleGen SeqCap EZ Exome

Library SR (Roche/Nimblegen, WI, USA) as per the manufacturer's protocol. Libraries were diluted in Qiagen Buffer EB (Qiaquick PCR Purification Kit) to a concentration of 6.5 pM. Next generation sequencing was performed (50 bp, paired end) on an Illumina HiSeq2000 with each sample exome library on a single lane of an Illumina TruSeq v2 flowcell (Illumina, CA, USA). Variants not shared between all affected individuals in the family studied, and variants that are non-autosomal, homozygous, and synonymous were excluded. Variants reported in SeattleSeq with a frequency of > 0.05% NHBLI Exome Sequencing Project (ESP) database (<http://evs.gs.washington.edu/EVS/>) were also excluded. Variants remaining after exome data analysis containing missing data were Sanger sequenced using the Big-Dye Terminator v3.1 chemistry (Applied Biosystems, CA), run on an ABI 3730xl analyzer, and analyzed using Sequencer software version 4.2 (Gene Codes, MI).

**Crystallization of AIF<sup>E493V</sup>.** AIF<sup>E493V</sup> was crystallized by a microbatch method under oil. The protein (0.6  $\mu$ l, 12 mg/ml) in 100 mM BisTris propane buffer, pH 7.5, was mixed with 0.6  $\mu$ l of the crystallization solution containing 30% polyethylene glycol 1500, 0.1 M Tris pH 8.5, and 4% acetone, and then covered with 10  $\mu$ l of paraffin oil. Crystals grew within several days at room temperature. X-ray diffraction data were collected at the Stanford Synchrotron Radiation Laboratory (SSRL) beamline 7-1 using paratone-N as a cryoprotectant. The structure was solved by molecular replacement with AIF<sup>wt</sup> (PDB code 1M6I) as a search model.

## Results

Charcot-Marie-Tooth disease (CMT) defines a clinically and genetically heterogeneous group of hereditary peripheral neuropathies characterized by chronic motor and sensory impairment. Charcot-Marie-Tooth disease is the most common hereditary neuromuscular disorder, with a prevalence of ~1 in 2,500 people.<sup>1</sup> Approximately 7-10% of CMT is inherited as an X-linked trait (CMTX).<sup>2,3</sup> Among the five known CMTX loci, the causal genes have been identified only for CMTX1 (MIM \*304040)<sup>4</sup> and CMTX5 (MIM \*311850).<sup>5</sup>

In 1985 Cowchock et al reported a large Italian-American family with a slowly progressive, childhood-onset, X-linked recessive axonal motor and sensory neuropathy associated with deafness and cognitive impairment.<sup>6</sup> By linkage analysis, the disease locus was mapped to an 11 cM region at chromosome Xq24-q26 (CMTX4 [MIM \*310490]).<sup>7,8</sup> We recently re-evaluated this family and identified a mutation in a candidate gene in this interval. The subjects were enrolled in an institutional review board approved protocol of the National Institute of Neurological Disorders and Stroke (NINDS), and informed consent was obtained from all living subjects.

The most consistently observed clinical abnormalities were distal muscle wasting, weakness, and sensory loss, with lower greater than upper limb involvement. Only males displayed the phenotype, consistent with an X-linked recessive mode of inheritance (Figure 1A). As described previously,<sup>6</sup>

electrophysiological studies in affected individuals showed evidence of motor more than sensory axonal neuropathy. Bilateral sensorineural hearing loss was also present in three subjects. Diminished intellectual abilities had been noted in several affected individuals since childhood.

Laboratory investigations in two affected individuals (III-6 and III-9) showed elevation of serum transaminases (up to 2x), lactate dehydrogenase (up to 440 U/L, normal values 113-226), and creatine kinase (up to 1169 U/L, normal values 52-386). Blood pyruvate and free and total carnitine were normal. Cranial MRI in two subjects (III-3 and III-9) showed multiple punctate T2 hyperintensities in the supratentorial white matter (Figure 1B). Muscle biopsy (left biceps; subject III-9) showed modest signs of neurogenic atrophy (Figure 1C-E), with no ragged-red fibers by modified Gomori trichrome staining and no abnormalities in histochemical staining for cytochrome oxidase and succinate dehydrogenase (not shown). Electron microscopy showed an increased number of mitochondria mainly in the subsarcolemmal areas, with moderate abnormality of mitochondrial shape and internal structure (Figure 1F).

We performed exome capture on one patient using SureSelect Human All Exome Kit v.1 (Agilent Technologies Inc.) and sequencing using a Genome Analyzer IIx (Illumina Inc.). The exome sequencing covered 74.3% of targeted regions with a read depth >20 x. Read alignment was performed to the human genome assembly hg19. We filtered variants to exclude HapMap SNPs present in dbSNP132 that had

an average heterozygosity greater than 0.02. This approach left a single candidate variant within the disease locus at position g.129,265,745, which predicts a c.1478A>T change (p.Glu493Val) in the *AIFM1* gene (MIM \*300169).

To confirm the *AIFM1* mutation, we used Sanger sequencing to screen 5 affected (II-3, III-3, III-5, III-7, and III-9) and 9 unaffected (I-1, I-2, II-1, II-2, II-5, II-8, III-2, and III-4) family members (Figure 1A). All clinically affected subjects were hemizygous and all mothers of affected individuals were heterozygous for the c.1478A>T (p.Glu493Val) variant (Figure 1G). None of the other unaffected subjects had this variant. Thus, the mutation in *AIFM1* completely co-segregated with the CMT phenotype. The Glu-493 residue is conserved across multiple species (Figure 1H), and the Val-493 variant was absent in 712 control individuals in the ClinSeq<sup>TM</sup> cohort.<sup>9</sup> No mutation in *AIFM1* was found in 102 unrelated males with CMT of unknown genetic cause.

AIF, a phylogenetically conserved mitochondrial flavoprotein, is one of the key caspase-independent death effectors.<sup>10-12</sup> The AIF precursor protein is a nuclear-encoded 67 kDa polypeptide, which, after cleavage of the N-terminal mitochondrial targeting sequence, is post-translationally inserted into the inner mitochondrial membrane, with the N-terminus facing the matrix and the C-terminal catalytic domain exposed to the intermembrane space.<sup>13</sup> Upon apoptotic insult, the membrane linker of AIF is cleaved off, and a soluble 57 kDa C-terminal fragment is released into the cytosol and transported into the nucleus, where it triggers

caspase-independent apoptosis with chromatin condensation and DNA fragmentation.<sup>10</sup> While the apoptotic function of AIF has been extensively investigated, the physiological role of the protein in normal mitochondria remains unclear. AIF has been proposed to function as a superoxide-generating NADH oxidase or electron transferase.<sup>14,15</sup> Despite recent *in vivo* analyses of the metabolic changes caused by AIF deficiency or defects, neither the substrates nor the acceptor(s) of its redox activity have been identified thus far. When its co-factor FAD is incorporated, the protein has a 100-fold preference for NADH over NADPH and forms dimeric FADH<sup>-</sup>-NAD charge-transfer complexes (CTCs), which are inefficient for electron transfer. Formation of CTC reduces the susceptibility of the N-terminus to proteolysis and weakens the AIF-DNA interaction, two events critical for initiation of caspase-independent apoptosis.<sup>16,17</sup> Further studies have suggested that AIF may act as a redox sensor with interrelated physiologic and apoptotic functions.<sup>18</sup> Insight into the normal function of AIF comes from the Harlequin (Hq) mouse, a spontaneous model of AIF deficiency due to retroviral insertion into the *Aifm1* gene.<sup>19</sup> The Hq model has 80% reduction in normal AIF expression, and decreased complex I and III activities in affected tissues, suggesting that AIF may control the biogenesis and maintenance of the respiratory complexes.<sup>20,21</sup> Recently, a c.del601-603 *AIFM1* mutation predicted to cause p.Arg201del was reported in two male infants with severe progressive mitochondrial encephalomyopathy, multiple defects of the respiratory chain activities, and increased caspase-independent apoptosis.<sup>22</sup> A second pathological *AIFM1* mutation, c.923G>A, which

predicts p.Gly308Glu, was associated with prenatal ventriculomegaly and infantile encephalomyopathy, primarily due to defects in the mitochondrial respiratory chain.<sup>23</sup> Gly-308 is located in a conserved NADH-binding region, suggesting that this function may be compromised by the p.Gly308Glu substitution.

The negatively-charged residue Glu-493 mutated in the family reported here is not directly involved in FAD- or NADH-binding but is only 10 Å away from the isoalloxazine ring that is the redox moiety of FAD. In oxidized AIF, Glu-493 is buried and assists in folding of the C-terminal regulatory insertion by mediating water-bridged contacts between the 532-534 and 581-584 peptides (Figure 2A, B). The Glu493Val mutation may weaken these interactions and lead to a more unstable protein conformation. In NADH-reduced AIF, the region surrounding Glu-493 becomes exposed to solvent.<sup>16</sup> As seen in Figure 2C, this surface is highly charged, with several acidic residues clustering near the pyrimidine portion of the isoalloxazine ring. This charge distribution is known to define the redox potential of FAD and, consequently, the flavoprotein reactivity. The x-ray structure of oxidized p.Glu493Val AIF shows that this substitution at position 493 does not affect protein folding but perturbs the electrostatic surface potential near the redox center and changes the surface profile (Figure 2D-F). This, in turn, could increase solvent accessibility of FAD and affect the redox reactivity of AIF.

To better understand the pathogenicity of the p.Glu493Val mutation identified in the family with CMTX, several properties of the recombinant mutant protein were

analyzed and compared to those of the wild type AIF and the previously reported p.Arg201del variant.<sup>22</sup> The absorbance spectrum, extinction coefficient, and midpoint redox potential of AIF were not affected by the p.Glu493Val mutation. Similar to the wild type AIF, p.Glu493Val AIF has high affinity for NADH, binds the cofactor tightly and in a stoichiometric fashion, and forms CTC upon reduction (Figure 3A). This implies that the NADH binding site in p.Glu493Val AIF is preserved. Nevertheless, we observed different circular dichroism spectra, higher flavin fluorescence, and a distinct proteolytic pattern of p.Glu493Val AIF (Supplemental Figure 1A-C), indicating structural dissimilarities between wild type and mutant proteins.

The most notable changes caused by the p.Glu493Val substitution were observed in electron transfer ability. First, p.Glu493Val AIF has lower  $K_M$  for NADH (by 20%) than wild type AIF, and becomes reduced by NADH 4-fold faster (Figure 3B and Table 1). Second, the dimeric CTC produced by wild type AIF reacts with oxygen slowly and is relatively stable,<sup>18</sup> whereas the half-life ( $t_{1/2}$ ) of CTC produced by p.Glu493Val AIF is one eighth that produced by the wild type protein (Figure 3C, Table 1). Since p.Glu493Val AIF retains its ability to dimerize upon reduction with NADH (Supplemental Figure 1D), an effect of the p.Glu493Val substitution on redox-linked dimer formation can be ruled out. Finally, p.Glu493Val AIF more efficiently transfers electrons to small electron-accepting molecules and cytochrome c (compare the  $k_{cat}/K_M^{NADH}$  values in Table 1, which reflect the enzyme

efficiency), but these redox reactions are partially uncoupled (~10% for p.Glu493Val AIF vs. 1-2% for wild type AIF).

Another distinct feature of p.Glu493Val AIF is the pH-dependence of its reaction with NADH. Unlike wild type AIF, which accepts the hydride atom from NADH in a pH-independent manner, the rate of p.Glu493Val AIF reduction is notably affected and increases by 6-fold at higher pH (Figure 3D). Such pH dependence indicates that reduction of p.Glu493Val AIF is associated with proton consumption, and may lead to the formation of a neutral FAD hydroquinone (FADH<sub>2</sub>). The latter redox species is less thermodynamically stable than an anionic hydroquinone (FADH<sup>-</sup>) formed by wild type AIF, which may be the reason for faster oxidation of p.Glu493Val AIF by electron acceptors. Based on these experimental data, we conclude that the Glu-493 residue controls proton accessibility to the flavin moiety and modulates the redox reactivity of AIF.

Importantly, the destabilization and faster oxidation of the p.Glu493Val AIF - NADH complexes *in vivo* can determine the accumulation of AIF monomers that are more prone to N-terminal proteolysis and release of the soluble, apoptogenic fragment.<sup>16,18</sup> Similar to p.Arg201del AIF,<sup>22</sup> the truncated apoptogenic form of p.Glu493Val AIF has higher affinity for DNA than the wild type protein (Figure 3E). The lack of an inhibiting effect of NADH on the p.Glu493Val AIF-DNA interaction, which is observed for wild type AIF,<sup>18</sup> was likely due to rapid and complete oxidation of p.Glu493Val AIF before the gel retardation experiment was over.

We then investigated the consequences of the p.Glu493Val mutation in patient-derived cultured skin fibroblasts and skeletal muscle. We first showed that the levels of mutant AIF in fibroblasts from patient III-3 were similar to those of wild type AIF in control cells (Figure 4A). Next, in order to test whether the p.Glu493Val AIF variant is directly linked to impaired oxidative phosphorylation, we analyzed the activity of the respiratory chain complexes in mutant fibroblast cell lines grown for 48 hrs in a galactose-rich (5 mM), glucose-free medium, a condition that forces cells to rely for energy on mitochondrial respiration rather than glycolysis. The activity of respiratory chain complexes in patient's fibroblasts was not reduced compared to carrier and controls (not shown). Likewise, no impairment in the respiratory chain activities was detected in a muscle biopsy from patient III-9 (not shown). In order to detect DNA fragmentation, which is a hallmark of apoptosis, we performed TUNEL assay in muscle biopsy. Numerous apoptotic cells were present in the patient's sample, whereas little to no staining was detected in healthy control muscle (Figure 4B).

Since AIF is a caspase-independent death effector, we treated p.Glu493Val AIF mutant and wild type AIF control fibroblasts with staurosporine (1 mM for 2 hr), a protein-kinase C inhibitor that induces cell death through the intrinsic, mitochondria-mediated pathway. We observed a much higher number of morphologically altered nuclei in staurosporine-treated p.Glu493Val AIF fibroblasts as compared to wild type AIF cells (Figure 4C). In cells pretreated with the general

caspase inhibitor z-VAD-FMK (100  $\mu$ M for 1/2 hr), the staurosporine-induced nuclear abnormalities dropped to less than 10% in control fibroblasts, but remained as high as 50% in p.Glu493Val AIF mutant cells (Figure 4C), suggesting prominent activation of the caspase-independent, AIF-specific cell death pathway.

In order to gain insight into p.Glu493Val AIF localization *in vivo*, 8  $\mu$ m muscle slices from patient III-9 and a healthy control were immunostained for AIF. Interestingly, more AIF-positive nuclear inclusions were detected in the patient's muscle than in the control, indicating that mutant p.Glu493Val AIF has higher propensity to translocate into the nucleus (Figure 4D).

In conclusion, we found that a missense mutation in *AIFM1* causes Cowchock syndrome, a form of X-linked recessive axonal motor and sensory neuropathy with sensorineural hearing loss and cognitive impairment. According to our analysis, p.Glu493Val AIF has slight structural changes and an abnormal propensity to NADH reduction and O<sub>2</sub> oxidation, likely due to changes in the FAD protonation state. Faster oxidation of p.Glu493Val AIF could lead to accumulation of AIF monomers, which translocate into the nucleus, where they trigger caspase-independent apoptosis. Interestingly, compared to the previously described p.Arg201del mutation,<sup>22</sup> the variant reported here alters the structure and redox properties of AIF to a milder extent (Figure 3B-D and table 1), which is consistent with a less severe clinical phenotype. Also, while oxidative phosphorylation (OXPHOS) failure is thought to play a major role in the pathophysiology of the p.Arg201del AIF-related

syndrome,<sup>22</sup> the mechanism of damage in CMTX4 appears to be OXPHOS-independent and primarily mediated by increased caspase-independent apoptosis.

Our identification of *AIFM1* as a gene mutated in CMT considerably broadens the phenotypic spectrum associated with *AIFM1* mutations. The results presented here also shed new light on the multiple pathogenic mechanisms in AIF-related diseases.

Analysis of additional *AIFM1* mutations may help to further unravel the pathophysiology of AIF defects, to identify proteins dependent on AIF activity, and to determine the exact role of AIF in mitochondria. Considering the wide range and importance of the cellular processes regulated by AIF, better understanding of AIF functions may have broad and unexpected implications in both medicine and cell biology.

### **Acknowledgments**

We are grateful to the family members for their participation and to Dr. Justin Y. Kwan, at NINDS, for performing the muscle biopsy. This work was supported in part by NINDS and NHGRI intramural research funding; National Institutes of Health Grant GM67637; the Pierfranco and Luisa Mariani Foundation, Italy; Fondazione Telethon grants GGP11011 and GPP10005; CARIPO grant 2011/0526; and the Italian Association of Mitochondrial Disease Patients and Families (Mitocon).

**Web Resources**

The URL for data presented herein is as follows:

Online Mendelian Inheritance in Man (OMIM), <http://www.ncbi.nlm.nih.gov/Omim>

dbSNP, <http://www.ncbi.nlm.nih.gov/projects/SNP/>

## References

1. Skre, H. (1974). Genetic and clinical aspects of Charcot-Marie-Tooth's disease. *Clin. Genet.* 6, 98-118.
2. Pareyson, D., Marchesi, C. (2009). Diagnosis, natural history, and management of Charcot-Marie-Tooth disease. *Lancet Neurol.* 8, 654-667.
3. Boerkoel, C.F., Takashima, H., Garcia, C.A., Olney, R.K., Johnson, J., Berry, K., Russo, P., Kennedy, S., Teebi, A.S., Scavina, M., et al. (2002). Charcot -Marie-Tooth disease and related neuropathies: mutation distribution and genotype-phenotype correlation. *Ann. Neurol.* 51, 190-201.
4. Bergoffen, J., Scherer, S.S., Wang, S., Scott, M.O., Bone, L.J., Paul, D.L., Chen, K., Lensch, M.W., Chance, P.F., Fischbeck, K.H. (1993). Connexin mutations in X-linked Charcot-Marie-Tooth disease. *Science* 262, 2039-2042.
5. Kim, H.J., Sohn, K.M., Shy, M.E., Krajewski, K.M., Hwang, M., Park, J.H., Jang, S.Y., Won, H.H., Choi, B.O., Hong, S.H., et al. (2007). Mutations in PRPS1, which encodes the phosphoribosyl pyrophosphate synthetase enzyme critical for nucleotide biosynthesis, cause hereditary peripheral neuropathy

- with hearing loss and optic neuropathy (cmtx5). *Am. J. Hum. Genet.* *81*, 552-558.
6. Cowchock, F.S., Duckett, S.W., Streletz, L.J., Graziani, L.J., Jackson, L.G. (1985). X-linked motor-sensory neuropathy type-II with deafness and mental retardation: a new disorder. *Am. J. Med. Genet.* *20*, 307-315.
  7. Fischbeck, K.H., ar-Rushdi, N., Pericak-Vance, M., Rozear, M., Roses, A.D., Fryns, J.P. (1986). X-linked neuropathy: gene localization with DNA probes. *Ann Neurol.* *20*, 527-532.
  8. Priest, J.M., Fischbeck, K.H., Nouri, N., Keats, B.J. (1995). A locus for axonal motor-sensory neuropathy with deafness and mental retardation maps to Xq24-q26. *Genomics* *29*, 409-412.
  9. Biesecker, L.G., Mullikin, J.C., Facio, F.M., Turner, C., Cherukuri, P.F., Blakesley, R.W., Bouffard, G.G., Chines, P.S., Cruz, P., Hansen, N.F., et al. (2009). The ClinSeq Project: piloting large-scale genome sequencing for research in genomic medicine. *Genome Res.* *19*, 1665-1674.
  10. Susin, S.A., Lorenzo, H.K., Zamzami, N., Marzo, I., Snow, B.E., Brothers, G.M., Mangion, J., Jacotot, E., Costantini, P., Loeffler, M., et al. (1999). Molecular

- characterization of mitochondrial apoptosis-inducing factor. *Nature* 397, 441-446.
11. Joza, N., Susin, S.A., Daugas, E., Stanford, W.L., Cho, S.K., Li, C.Y., Sasaki, T., Elia, A.J., Cheng, H.Y., Ravagnan, L., et al. (2001). Essential role of the mitochondrial apoptosis-inducing factor in programmed cell death. *Nature* 410, 549-554.
  12. Lorenzo, H.K., Susin, S.A., Penninger, J., Kroemer, G. (1999). Apoptosis inducing factor (AIF): a phylogenetically old, caspase-independent effector of cell death. *Cell Death Differ.* 6, 516-524. Review.
  13. Otera, H., Ohsakaya, S., Nagaura, Z., Ishihara, N., Mihara, K. (2005). Export of mitochondrial AIF in response to proapoptotic stimuli depends on processing at the intermembrane space. *EMBO J.* 24, 1375-1386.
  14. Miramar, M.D., Costantini, P., Ravagnan, L., Saraiva, L.M., Haouzi, D., Brothers, G., Penninger, J.M., Peleato, M.L., Kroemer, G., Susin, S.A. (2001). NADH oxidase activity of mitochondrial apoptosis-inducing factor. *J. Biol. Chem.* 276, 16391-16398.

15. Maté, M.J., Ortiz-Lombardía, M., Boitel, B., Haouz, A., Tello, D., Susin, S.A., Penninger, J., Kroemer, G., Alzari, P.M. (2002). The crystal structure of the mouse apoptosis-inducing factor AIF. *Nat. Struct. Biol.* *9*, 442-446.
16. Sevrioukova, I.F. (2009). Redox-linked conformational dynamics in apoptosis-inducing factor. *J. Mol. Biol.* *390*, 924-938.
17. Sevrioukova, I.F. (2011). Apoptosis-inducing factor: structure, function, and redox regulation. *Antioxid. Redox Signal.* *14*, 2545-2579.
18. Churbanova, I.Y., Sevrioukova, I.F. (2008). Redox-dependent changes in molecular properties of mitochondrial apoptosis-inducing factor. *J. Biol. Chem.* *283*, 5622-5631.
19. Klein, J.A., Longo-Guess, C.M., Rossmann, M.P., Seburn, K.L., Hurd, R.E., Frankel, W.N., Bronson, R.T., Ackerman, S.L. (2002). The harlequin mouse mutation downregulates apoptosis-inducing factor. *Nature* *419*, 367-734.
20. Vahsen, N., Candé, C., Brière, J.J., Bénit, P., Joza, N., Larochette, N., Mastroberardino, P.G., Pequignot, M.O., Casares, N., Lazar, V., et al. (2004). AIF deficiency compromises oxidative phosphorylation. *EMBO J.* *23*, 4679-4689.

21. Apostolova, N., Cervera, A.M., Victor, V.M., Cadenas, S., Sanjuan-Pla, A., Alvarez-Barrientos, A., Esplugues, J.V., McCreath, K.J. (2006). Loss of apoptosis-inducing factor leads to an increase in reactive oxygen species, and an impairment of respiration that can be reversed by antioxidants. *Cell. Death Differ.* *2*, 354-357.
  
22. Ghezzi, D., Sevrioukova, I., Invernizzi, F., Lamperti, C., Mora, M., D'Adamo, P., Novara, F., Zuffardi, O., Uziel, G., Zeviani, M. (2010). Severe X-linked mitochondrial encephalomyopathy associated with a mutation in apoptosis-inducing factor. *Am. J. Hum. Genet.* *86*, 639-649.
  
23. Berger, I., Ben-Neriah, Z., Dor-Wolman, T., Shaag, A., Saada, A., Zenvirt, S., Raas-Rothschild, A., Nadjari, M., Kaestner, K.H., Elpeleg, O. (2011). Early prenatal ventriculomegaly due to an AIFM1 mutation identified by linkage analysis and whole exome sequencing. *Mol. Genet. Metab.* *104*, 517-520.

## Figure legends

### **Figure 1. Pedigree, brain imaging and skeletal muscle analysis, and Sanger sequencing.**

(A) Pedigree of the family. White, unaffected; black, affected.

(B) Fluid-attenuated inversion recovery (FLAIR) magnetic resonance imaging on a transverse section of supratentorial brain of a patient showing multiple punctate hyperintensities in the white matter (subject III-6).

(C-E) Muscle biopsy showing variation in fiber size (hematoxylin and eosin staining, C), esterase positive angular atrophic myofibers (esterase staining, D), and fiber grouping with some targetoid fibers (nicotinamide adenine dinucleotide-tetrazolium reductase, E), and (subject III-9).

(D) Electron microscopic image of muscle showing variation in shape and increase in number of mitochondria, mainly in the subsarcolemmal areas (subject III-9).

(G) Chromatograms of AIFM1 showing the c.1478A>T (p.Glu493Val) variant (asterisk) in patient (hemizygote) and carrier (heterozygote).

(H) Protein homology of AIF in various species. The mutation results in amino acid substitutions at Glu493, a highly conserved residue.

**Figure 2. Structural comparison of the wild type and p.Glu493Val mutant of AIF.**

The E493V substitution was introduced into the human AIF1 expression plasmid using Stratagene QuikChange kit. Expression, purification, and removal of the C-terminal six-histidine affinity tag were carried out as described previously.<sup>18</sup>

(A) Position of Glu493 (indicated by an arrow) in oxidized human AIF<sup>wt</sup> (PDB code 1M6I). FAD is shown in yellow and a partially disordered regulatory peptide is in pink.

(B) Water-bridged contacts involving Glu493 hold the 512-533 helical fragment of the regulatory peptide (pink) close to the active site.

(C) Charge distribution near the flavin cofactor. Positively and negatively charged residues are depicted in blue and red, respectively. Glu493 is 10 Å away from FAD and is part of an acidic cluster adjacent to the isoalloxazine ring.

(D) Superposition of the structures of the wild type (gray, PDB code 1M6I) and Glu493Val mutant of human AIF (green, PDB code 4FDC). The structure of AIF<sup>E493V</sup> was solved at 2.4 Å resolution. Data collection and refinement statistics are given in Supplemental Table 1. The valine side-chain is shown in cyan.

(E) A magnified view at the region of AIF near the site of the p.Glu493Val substitution demonstrating that the mutation does not alter the structure near the active site of AIF.

(F) The Glu493Val mutation changes both the surface profile and electrostatic potential, which may affect solvent accessibility and redox properties of FAD.

**Figure 3. Comparison of the redox and molecular properties of the wild type and p.Glu493Val and p.Arg201del mutants of AIF.**

(A) Anaerobic titration of AIF<sup>E493V</sup> with NADH. Similar to the wild type protein, the p.Glu493Val variant binds NADH tightly and produces a FADH<sup>-</sup>-NAD charge-transfer complex (CTC) absorbing in the long-wavelength region. Inset shows that an equimolar amount of NADH is required to fully reduce FAD.

(B) Kinetics of AIF reduction with NADH. Proteins were mixed with NADH in a stopped flow spectrophotometer, and reduction of FAD was monitored at 452 nm. The derived kinetic parameters are given in Table 1.

(C) Kinetics of oxidation of NADH-reduced AIF. Proteins were reduced with a 4-fold excess of NADH before exposure to atmospheric oxygen. Flavin oxidation was monitored at 452 nm.

(D) Effect of pH on the kinetics of AIF reduction with NADH.

(E) Comparison of DNA binding by wild type and mutant AIF. Proteins were incubated for 15 min with 250 ng of 100 bp DNA ladder (New England Biolabs) in the absence and presence of a 20-fold excess of NADH. After separation on a 2% agarose gel, DNA was visualized with ethidium bromide. Lane 1 is a control (DNA only).

**Figure 4. The p.Glu493Val mutant induces caspase-independent apoptosis.**

(A) Western blot analysis of patient (Mt) and control (Ct) skin cultured fibroblasts, immunodetected with an antibody against AIF (Chemicon). Antibody against subunit A of complex II (SDHA, Invitrogen) was used as loading control.

(B) TUNEL and DAPI staining of skeletal muscle nuclei from patient (Pt) and control (N). A normal biopsy treated with DNase was used as a positive control (Ct). Numerous TUNEL-positive nuclei are present in the patient (Pt), whereas no TUNEL positive nuclei are seen in the control (N).

(C) Quantification of altered nuclei in control fibroblasts (Ct) and in fibroblasts from patient (Mut) after treatment with staurosporine (Stau) (1 mM for 2 hr) in presence or absence of Z-VAD-fmk (Z) (100  $\mu$ M for 1/2 hr).

(D) AIFM1 (1:1000; Millipore, AB16501) immunostaining of cross section of muscle biopsy showing nuclear localization of mutant AIF in a patient hemizygous for p.Glu493Val (E493V) compared to control (wt). Nuclei were counterstained with DAPI.

## Figures

Figure 1

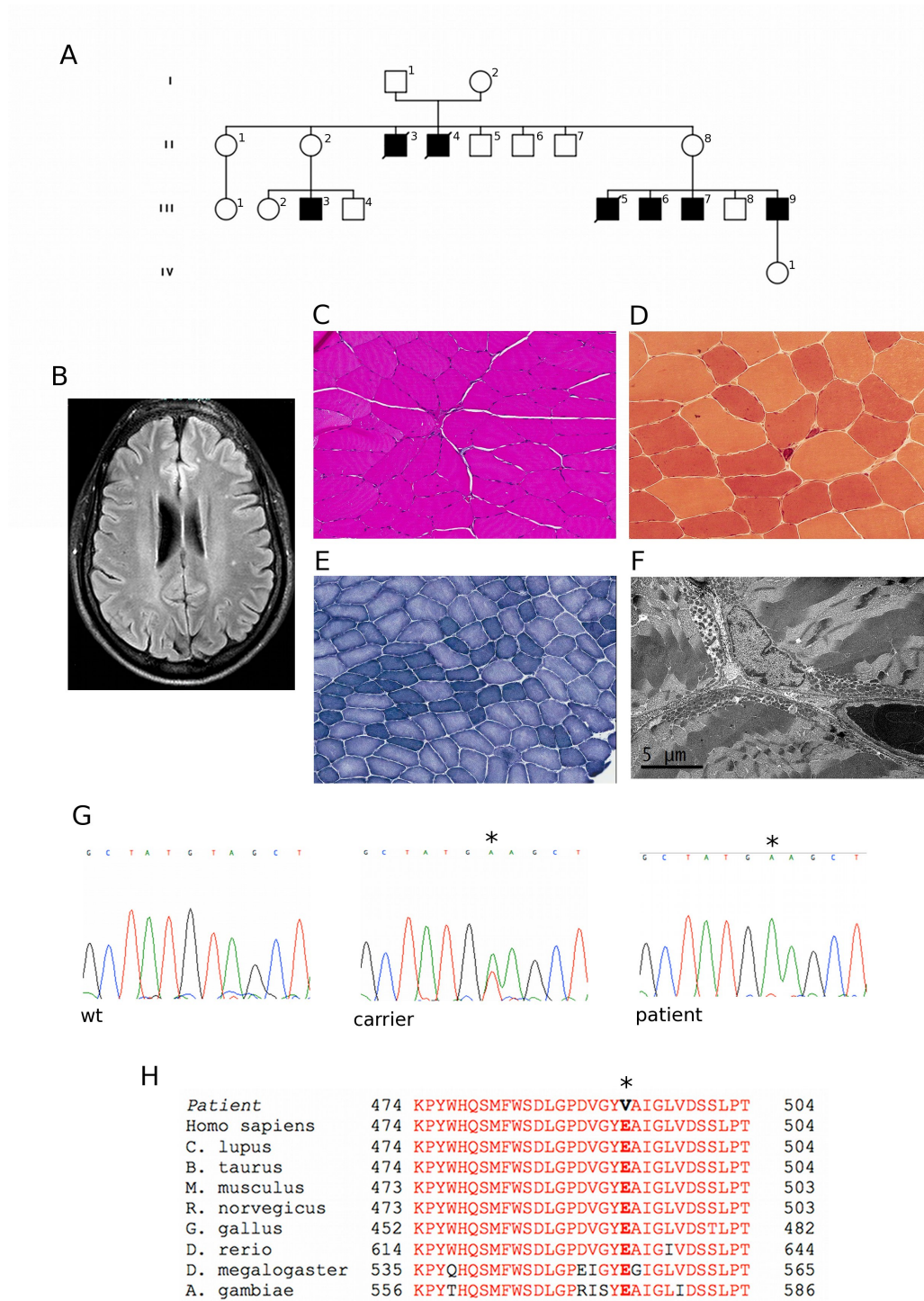


Figure 2

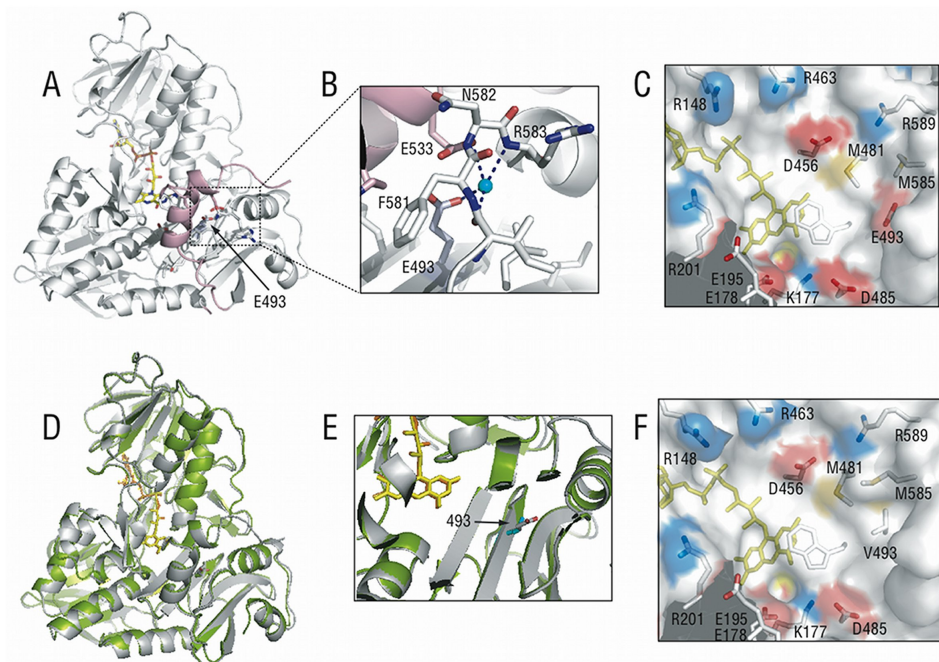


Figure 3

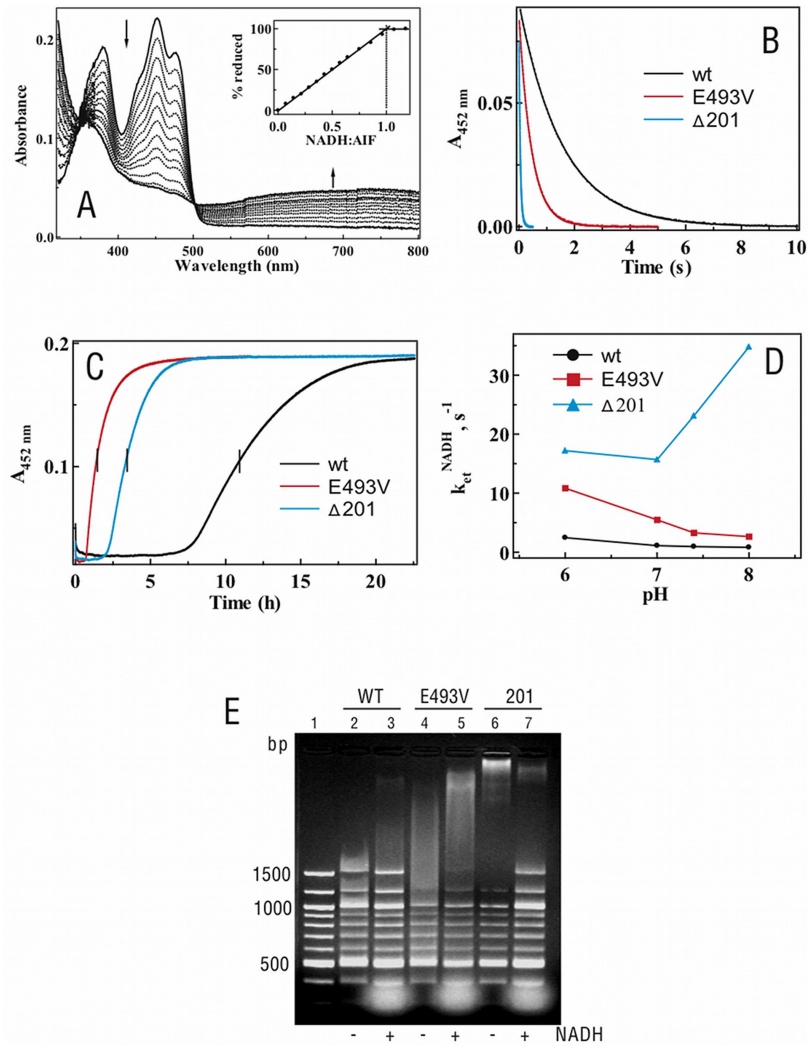
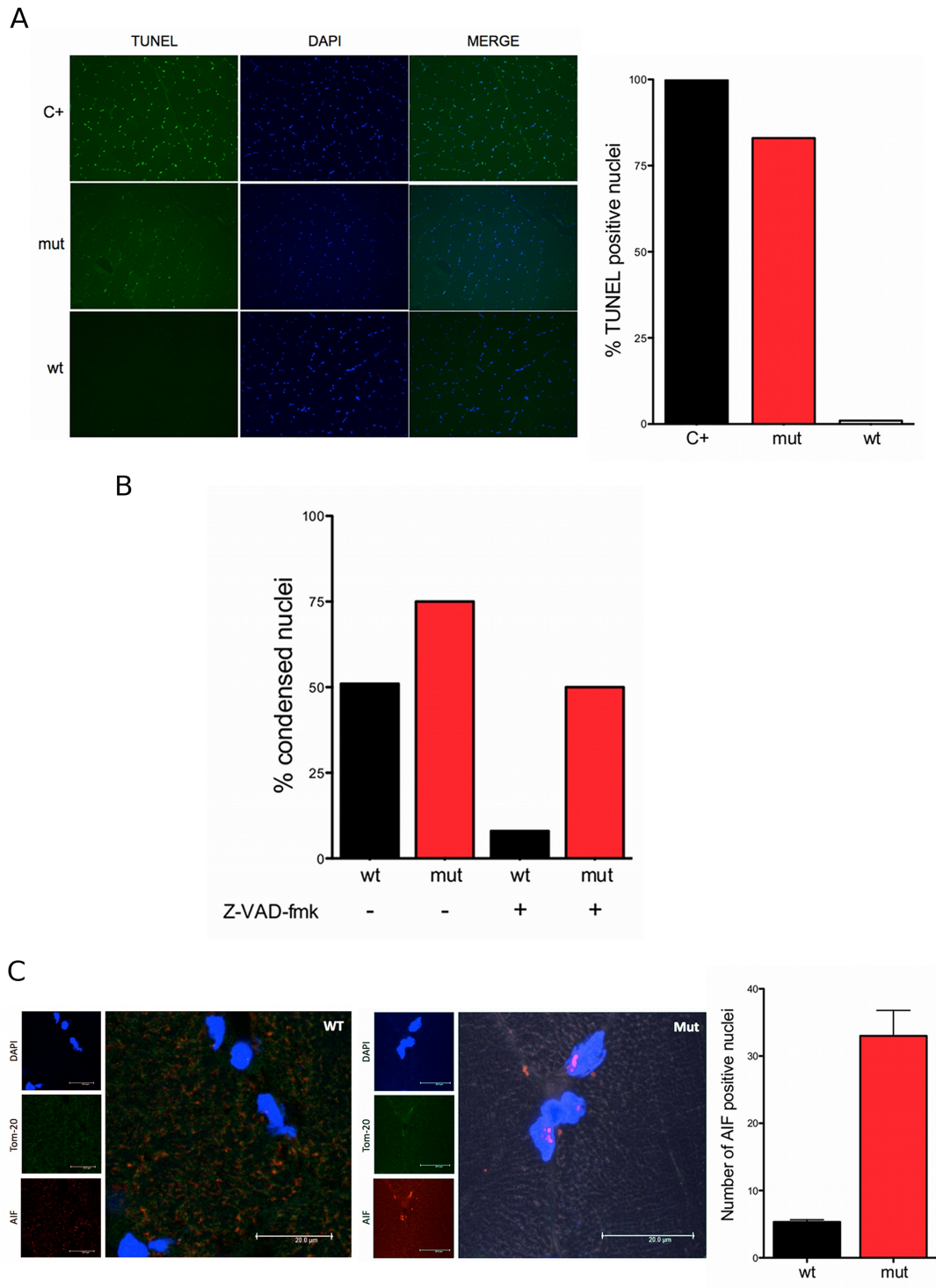


Figure 4

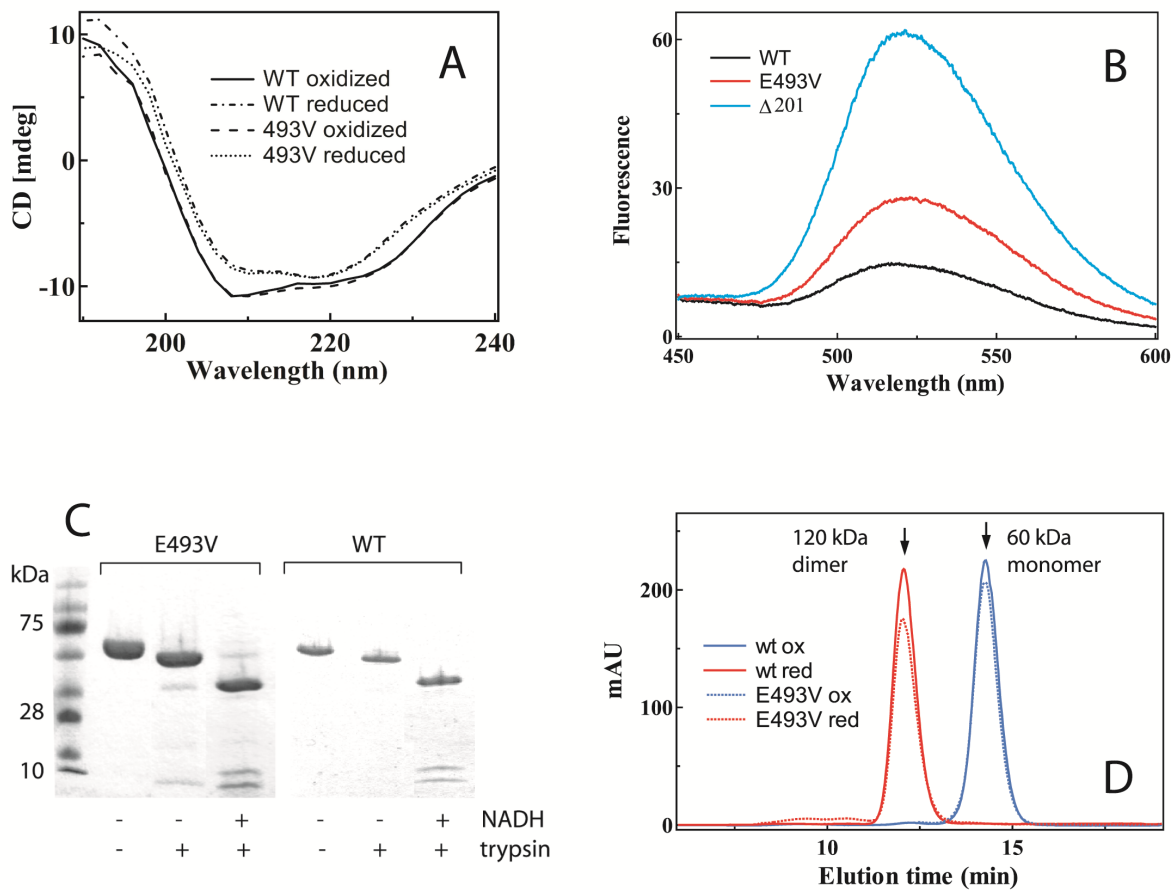


**Table**

Table 1. Redox properties and activities of the wild type and mutants of mature human AIF			
	WT	E493V	$\Delta$ R201
$k_{\text{et}}^{\text{NADH}}$ ( $\text{s}^{-1}$ ) <sup>a</sup>	0.98 ± 0.02	3.9 ± 0.1	23 ± 0.4
$K_{\text{M}}^{\text{NADH}}$ (mM)	1.53 ± 0.06	1.23 ± 0.05	0.23 ± 0.02
$t_{1/2}^{\text{CTC}}$ (h) <sup>b</sup>	11	1.4	3.4
$k_{\text{ox}}^{\text{NADH}}$ ( $\text{min}^{-1}$ ) <sup>c</sup>	0.015 ± 0.002	0.12 ± 0.02	0.06 ± 0.01
<b>DCIP</b>			
$k_{\text{cat}}$ ( $\text{min}^{-1}$ )	137 ± 18	335 ± 32	394 ± 28
$K_{\text{M}}^{\text{DCIP}}$ ( $\mu\text{M}$ )	202 ± 36	97 ± 20	16 ± 3
$K_{\text{M}}^{\text{NADH}}$ (mM)	0.74 ± 0.12	0.16 ± 0.04	0.14 ± 0.02
$k_{\text{cat}}/K_{\text{M}}^{\text{NADH}}$	185	2,094	2,814
<b><math>K_3\text{Fe}(\text{CN})_6</math></b>			
$k_{\text{cat}}$ ( $\text{min}^{-1}$ )	314 ± 25	745 ± 30	1,464 ± 92
$K_{\text{M}}^{K_3\text{Fe}(\text{CN})_6}$ ( $\mu\text{M}$ )	28 ± 5	26 ± 5	68 ± 6
$K_{\text{M}}^{\text{NADH}}$ (mM)	0.61 ± 0.10	0.26 ± 0.05	0.20 ± 0.03
$k_{\text{cat}}/K_{\text{M}}^{\text{NADH}}$	515	2,865	7,320
<b>Cytochrome c</b>			
$k_{\text{cat}}$ ( $\text{min}^{-1}$ )	54 ± 15	35 ± 5	39 ± 2
$K_{\text{M}}^{\text{cyt c}}$ ( $\mu\text{M}$ )	26 ± 13	28 ± 8	94 ± 10

$K_M^{\text{NADH}}$ (mM)	$0.27 \pm 0.02$	$0.15 \pm 0.02$	$0.07 \pm 0.01$
$k_{\text{cat}}/K_M^{\text{NADH}}$	200	233	557
<p><sup>a</sup> The rate constant for the AIF reduction with NADH determined by stopped flow spectrophotometry at 25°C.</p> <p><sup>b</sup> The half-lifetime of the FADH<sub>2</sub>-NAD charge-transfer complex (CTC) was determined at 25°C in the presence of 15 μM AIF and 60 μM NADH.</p> <p><sup>c</sup> The rate of NADH oxidation by AIF was determined at 25°C.</p> <p>All activities were determined in 50 mM phosphate buffer, pH 7.4, at 25°C as reported elsewhere (Churbanova, 2008).</p>			

## Supplemental Data

**Supplemental Figure 1. Effect of the E493V mutation on the molecular properties**

**of AIF.** (A) Circular dichroism (CD) spectra indicate that replacement of Glu493 with valine induces only subtle changes in the AIF structure. Far UV CD spectra were recorded in the absence and presence of a 20-fold excess of NADH.

(B) Flavin fluorescence in the wild type and mutant AIF. FAD is buried and virtually non-fluorescent in AIF<sup>wt</sup>. 2- and 5-fold increases in flavin fluorescence in the E493V

and  $\Delta 201$  mutants, respectively, indicate higher solvent accessibility or partial exposure of FAD.

(C) Tryptic digest of oxidized and NADH-reduced AIF<sup>E493V</sup> and AIF<sup>wt</sup>. Oxidized AIF<sup>wt</sup> undergoes proteolysis only at the Arg126-Ala127 site and runs on the SDS PAGE gel as a single band of ~50 kDa. The digest pattern indicates that, unlike in AIF<sup>wt</sup>, the C-terminal regulatory insertion in the E493V mutant is partially unfolded and accessible to trypsin. (D) Redox-dependent monomer-dimer transition in AIF<sup>E493V</sup> is not perturbed.

**Supplemental Table 1.****Data collection and refinement statistics*****Data statistics***


---

Space group	C2
Unit cell parameters	$a = 102 \text{ \AA}, b = 63 \text{ \AA}, c = 102 \text{ \AA};$ $\alpha, \beta = 90^\circ; \gamma = 119^\circ$
Resolution range	39.5 – 2.4 (2.40 – 2.46) <sup>a</sup>
<b>Total reflections</b>	<b>148410 (1427)</b>
Unique reflections	20005 (1308)
Redundancy	6.8 (6.8)
Completeness	94.2 (88.7)
Average $I/\sigma$	11.3 (3.1)
R <sub>merge</sub>	0.075 (0.45)

***Refinement statistics***

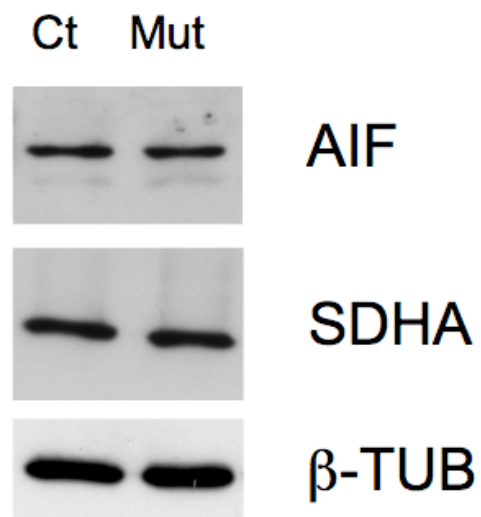
Molecules per asymmetric unit	1
$R/R_{\text{free}}^b$	25.5/29.7

**r.m.s. deviations**

Bond lengths, $\text{\AA}$	0.007
Bond angles, $^\circ$	1.2

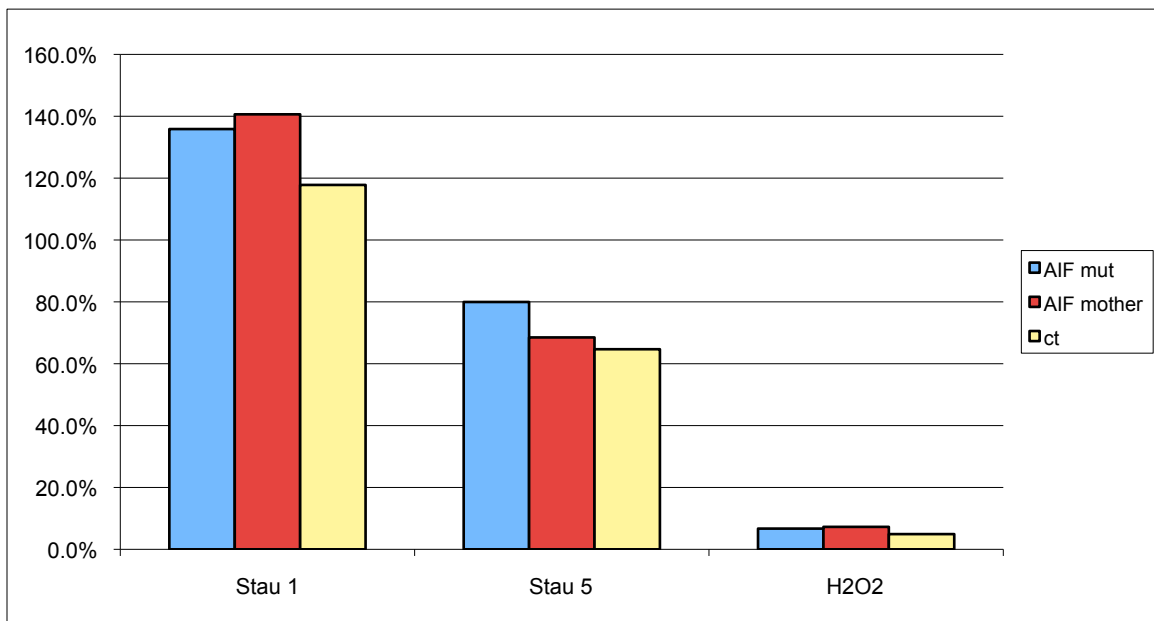
---

<sup>a</sup> Values in brackets are for the highest resolution shell.



**Supplemental Figure 2.** Western blot analysis of patient (Mt) and control (Ct) skin cultured fibroblasts, immunodetected with an antibody against AIF (Chemicon).

Antibodies against subunit A of complex II (SDHA, Invitrogen) and  $\beta$ -tubulin (Sigma) were used as loading controls.



**Supplemental Figure 3.** The viability of fibroblasts from affected (AIF mut), carrier (AIF mother) and control (ct) subject was assessed using CyQUANT Direct Cell Proliferation Assay (Invitrogen). Cells were treated for 2 hours with staurosporine 1 $\mu$ M (Stau 1), 5  $\mu$ M (Stau 5), or hydrogen peroxide (H2O2) 15 mM.

**Chapter 2-1**

**Spinal and bulbar muscular atrophy: from disease pathogenesis to clinical management.**

**Christopher Grunseich, Carlo Rinaldi and Kenneth H. Fischbeck**

Neurogenetics Branch, National Institute of Neurological Disorders and Stroke,

National Institutes of Health, Bethesda, MD, USA

## Introduction

Spinal and bulbar muscular atrophy (SBMA), also known as Kennedy's disease (Kennedy *et al*, 1968), is a slowly progressive disease with lower motor neuron loss and weakness, atrophy, and fasciculations. The disease is caused by a trinucleotide (CAG) repeat expansion in the androgen receptor (AR) gene on the X chromosome (La Spada *et al*, 1991), which results in an expanded polyglutamine tract and an androgen-dependent toxic gain of function in the mutant protein. The disease has been reported across many ethnicities, with an estimated prevalence of about 1 in 40,000. Normal individuals will have repeat lengths between 11 and 36 CAGs, and the disease will occur when this repeat length increases to between 38 and 62 CAGs (Atsuta *et al*, 2006; Rhodes *et al*, 2009). We report the case of a 29-year-old male with 68 CAGs (see Case Report. *In submission*). Although there is no treatment available to alter the progression of this disease, patients may have benefit from symptomatic treatment.

The precise mechanism by which the expansion results in motor neuron death is not clear, although several putative mechanisms have been investigated. The toxic gain of function of the AR is dependent on androgens such as testosterone and dihydrotestosterone. In addition to these toxic effects of the AR, evidence of loss of normal receptor function also contributes to the disease phenotype, with some patients experiencing gynecomastia and reduced fertility. The mutant AR is prone to aggregation (Walcott *et al*, 2002; Li *et al*, 1998), and its

effect on cellular signal transduction, mitochondria function, and axonal transport is likely to be contributing to the disease (McC Campbell *et al.*, 2000; Lieberman *et al.*, 2002; Ranganathan *et al.*, 2009; Katsuno *et al.*, 2006).

### **From AR functions to motor-neuron disease: pathophysiology of SBMA**

The cause of SBMA is an expansion of a trinucleotide CAG repeat, which encodes the polyglutamine tract, in the first exon of the androgen receptor (AR) gene (La Spada *et al.*, 1991). A similar gene mutation has been detected in Huntington's disease, dentatorubral-pallido-luysian atrophy (DRPLA), and several forms of spinocerebellar ataxias (Gatchel *et al.*, 2005). Since CAG is translated to glutamine, these disorders are called polyglutamine diseases. In SBMA, like in other polyglutamine diseases, there is an inverse correlation between the CAG repeat size and the age of onset, or the disease severity adjusted by the age of examination (Doyu *et al.*, 1992; Atsuta *et al.*, 2006).

Although the disease-causing proteins are expressed widely in the CNS, specific populations of neurons are vulnerable in each disease, resulting in characteristic patterns of neurodegeneration and clinical features (Zoghbi & Orr *et al.*, 2000).

In SBMA degeneration of anterior horn cells in the spinal cord of affected individuals is observed (Kennedy *et al.*, 1968; Ogata *et al.*, 1994). Some affected

males also experience degeneration of the dorsal root ganglia, leading to mild abnormalities in sensory function in the distal extremities (Sobue *et al.*, 1981; Nagashima *et al.*, 1988). Emerging evidence suggests that mutant AR may exert a direct toxic effect on skeletal muscle: histological and molecular signs of muscle pathology are detectable before the appearance of pathological abnormalities in the spinal cord in a knock-in mouse model of SBMA (Yu *et al.*, 2006), and analysis of muscle biopsy samples derived from SBMA patients suggests a mixed pathology with both myopathic and neurogenic features (Soraru *et al.*, 2008).

Unlike other polyglutamine diseases in which the function of the unexpanded protein is not clear, in SBMA the disease protein has a well-characterized role as a ligand-dependent transcription factor. AR is a member of the nuclear hormone receptor superfamily and resides in the cytoplasm when inactive, in a complex with heat-shock and heat-shock-related proteins. Upon binding with its natural ligands, testosterone and its more potent derivative dihydrotestosterone, a number of events occur, including AR posttranslational modification, nuclear translocation and DNA binding. These changes ultimately result in AR-mediated activation or repression of target genes. These changes occur in concert with conformational modifications that result in the exposure of two co-regulator interaction surfaces, termed activation function-1 (AF-1) and activation function-2 (AF-2) (Nedelsky *et al.*, 2010).

In SBMA as in other polyglutamine diseases, human and mouse genetic data

suggests that the disease mainly results from a gain-of-function mechanism, since AR gene deletion in humans does not lead to a motor neuron disease, and a mouse model employing expanded polyglutamine AR protein accurately reflect the human disease, displaying restricted symptoms, lower motor neuron specificity and gender specificity (Katsuno *et al.*, 2002). Nevertheless, a loss of normal AR function may also play a role in the pathogenesis, as suggested by the fact that some SBMA patients show mild signs of partial androgen insensitivity like gynecomastia and testicular atrophy.

A pathological hallmark of the polyglutamine diseases is the presence of intranuclear and/or cytoplasmic inclusions of the disease proteins that are ubiquitinated and often associated with various transcription factors, chaperones, and proteasome components (Li *et al.*, 1998). Since human AR is widely expressed in various organs, nuclear accumulation of the pathogenic AR protein is detected not only in the brain, but also in non-neuronal tissues such as kidney, skeletal muscle, adrenal gland, and scrotal skin. Although nuclear inclusions are a disease-specific histopathological finding, their role in the pathogenesis has been heavily debated. Several studies suggest that the monomers and soluble oligomers of the expanded protein constitute the toxic species in polyglutamine diseases and that the intranuclear inclusions may rather indicate a cellular response coping with the toxicity of abnormal polyglutamine protein (Arrasate *et al.*, 2004; Miller *et al.*, 2011).

Although the expansion might interfere with the normal function of the host protein, it is not yet clear how this contributes to pathogenesis. A number of studies have indicated that transcriptional dysregulation underlies the molecular mechanism of neuronal dysfunction in polyglutamine disease (McCampbell *et al.*, 2002; Minamiyama *et al.*, 2004). CREB-binding protein (CBP), a transcriptional co-activator that orchestrates the nuclear response to a variety of cell signaling cascades, is incorporated into nuclear inclusions formed by polyglutamine-containing proteins in cultured cells, transgenic mice, and tissue from patients with SBMA (McCampbell *et al.*, 2002). Histone acetylation is decreased in mouse model of SBMA, which may be a consequence of altered CBP localization (Minamiyama *et al.*, 2004). Mitochondrial impairment and oxidative stress have also been suggested as a causative molecular event in SBMA (Ranganathan *et al.*, 2009). Moreover, the pathogenic AR protein represses the transcription of the subunits of peroxisome proliferators-activated receptor gamma co-activator (PGC-1), a transcriptional co-activator that regulates the expression of various nuclear-encoded mitochondrial proteins (Ranganathan *et al.*, 2009). In the muscle of both the SBMA mouse model, and SBMA patients, neurofilaments and synaptophysin accumulate at the distal motor axon, suggesting an impairment of retrograde axonal transport (Katsuno *et al.*, 2006).

#### **Diagnostic studies and evaluation**

The diagnosis is usually made following genetic testing, with all affected individuals having a trinucleotide repeat expansion containing at least 38 CAGs in the first exon of the AR gene (La Spada *et al*, 1991). Aspartate and aspartate aminotransferases are found to be mildly elevated above the reference range, and creatine kinase is elevated in most subjects to the 900-1400 U/l range (Atsuta *et al*, 2006; Rhodes *et al*, 2009). SBMA subjects may also have impaired glucose tolerance, and elevation of the low-density lipoprotein levels above normal. Although most patients can have elevations in average total testosterone, free testosterone, and dihydrotestosterone, the levels of free testosterone and dihydrotestosterone may also be reduced in some individuals.

The key electrodiagnostic features on EMG/NCS will be low sensory nerve amplitudes, decreased compound motor action potentials, and evidence of diffuse denervation atrophy. Motor unit nerve estimation (MUNE) can be reduced to about half of healthy control values. A muscle biopsy is not needed to make a diagnosis, but can show evidence of neurogenic and myogenic atrophy (Kennedy *et al*, 1968; Soraru *et al*, 2008).

A majority of SBMA patients have a pertinent family history (Rhodes *et al*, 2009). Since SBMA is an X-linked recessive disease, the children of affected patients are asymptomatic. The disease may be passed through asymptomatic females, e.g., mothers, sisters, and daughters of affected patients. Female carriers do not develop weakness, and a small number may experience cramping (Ishihara

*et al*, 2001). The CAG repeat may change between generations, with longer repeats correlating to an earlier age of disease onset (La Spada *et al*, 1992). Carriers and those who are at risk of being carriers should have access to genetic counseling services.

### **Clinical Presentation**

Neurological features of the disease usually begin during the fourth or fifth decade of life, but the onset ranges from ages 18 to 64 (Rhodes *et al*, 2009). Initial symptoms can include tremor, cramping, and weakness (Dias *et al*, 2011 can't find the reference). The classic signs of lower motor neuron disease are typical, and include reduced deep tendon reflexes, atrophy, and fasciculations in the muscles of the extremities. Weakness will present as difficulty climbing stairs and walking, particularly long distances. The distribution of weakness is both proximal and distal, with asymmetry more frequently involving the dominant side (Rhodes *et al*, 2009). Degeneration of the dorsal root ganglia can result in a loss of sensory function in the distal extremities. Patients will also typically have evidence of androgen insensitivity, which can manifest as gynecomastia, oligospermia, and erectile dysfunction. The interruption of normal androgen receptor function has been shown to decrease the risk of androgenetic alopecia in SBMA (Sinclair *et al*, 2007).

Most individuals also show involvement of the bulbar muscles and have difficulty with speech articulation and swallowing (Figure 1). Dysarthria and dysphagia appear at a median age of 50 and 54 years, respectively (Astuta *et al.*, 2006). Other symptoms reported include weakness and atrophy primarily involving the facial and tongue muscles with perioral fasciculations (Figure 2; video), and changes in voice and speech, characterized by hypernasality and a decreased range of pitch and loudness. SBMA patients may present with fatigue when chewing and occasionally with jaw drop, caused by severe weakness of the jaw-closure muscles (temporalis and masseter muscles) with preservation of jaw-opening muscles (pterygoid muscles) (Sumner *et al.*, 2002).

The disease will usually progress slowly, and in a recent clinical trial a 2% decline in muscle strength per year was detected using quantitative muscle assessment (Fernandez-Rhodes *et al.*, 2011).

The vast majority of individuals with SBMA have a normal life expectancy and do not die from direct complications of the disease. About 10% of affected individuals are at risk for asphyxiation or aspiration pneumonia because of weakness of the bulbar musculature (Kennedy *et al.*, 1968; Astuta *et al.*, 2006). This is the only life-threatening complication in SBMA.

Dysarthria, dysphagia, and the onset age of pneumonia significantly correlates with the number of CAG repeats (Astuta *et al.*, 2006). Since bulbar symptoms most strongly affect prognosis, videofluorography-assessed pharyngeal barium residue

has been used as primary or secondary outcome measure in SBMA clinical trials (Katsuno *et al.*, 2010; Fernandez-Rhodes *et al.*, 2011).

### **Differential Diagnosis**

The diagnosis of SBMA is delayed for many patients due to decreased awareness of the disease. With the availability of genetic testing, and recognition of the key characteristic clinical features, a diagnosis can be relatively straightforward. The time to diagnosis will typically be postponed for 5.5 years on average, and subjects will wait 3.5 years from the onset of weakness to the time they are first medically evaluated (Rhodes *et al.*, 2009). If a misdiagnosis occurs, SBMA patients are most likely initially diagnosed with amyotrophic lateral sclerosis (ALS). Dysphagia and dysarthria are a common finding in ALS; nevertheless, differentiation of ALS from SBMA can usually be made based on history and physical examination. Individuals with ALS usually display upper and lower motor neuron signs as well as a more rapid disease progression. Jaw drop, jaw and orbicularis oris weakness, and ptosis in middle-aged men are more frequently associated with myasthenia gravis. However, negative antiacetylcholine receptor antibody, together with lack of improvement with MG specific therapies (pyridostigmine, corticosteroids or other immunosuppressants) can help in the diagnosis. It is common for people with different myopathies (i.e. myotonic dystrophy or facioscapulohumeral muscular dystrophy) to develop a nasal voice and swallowing problems. Some suffer

weakness in their diaphragm and chest muscles, which results in breathing problems. Electrophysiology, serum CK concentration, and/or muscle biopsy are often warranted to differentiate the disease from motor neuron disease..

## **Management**

There is currently no treatment available to alter the course of the disease. Animal models can recapitulate some aspects of the disease phenotype, and androgen reduction therapy in these animals has been effective (Katsuno *et al*, 2003). Testing of the androgen reducing agents leuprorelin and dutasteride in placebo controlled, randomized, clinical trials has not shown significant effects on the primary outcome measures (Fernandez-Rhodes *et al*, 2011; Banno *et al*, 2009; Katsuno *et al*, 2010). SBMA management should be focused on enhancing mobility and function while also preventing complications of the disease. Subjects who describe choking spells or dysphagia should undergo a speech and swallow evaluation to evaluate for bulbar dysfunction. Behavioral changes can be instituted to reduce the risk of aspiration. While dyspnea is not typically encountered in SBMA, pulmonary function testing should be done in those subjects experiencing shortness of breath. Mobility and ambulation can be enhanced with a physical therapy evaluation to identify those patients who may benefit from braces and assistive devices.

The effect of activity level on function in SBMA remains uncertain. A study of moderate-intensity aerobic exercise in eight SBMA subjects by Preisler *et al.* showed mixed results with an increase in maximal work capacity, but no effect on maximal oxygen uptake. Given the variability in function across the SBMA population, exercise needs to be tailored to the patient's level of function. Although we would expect exercise to help maintain and improve mobility, more studies are needed to assess whether functional exercise may be beneficial.

## References

1. Arrasate M, Mitra S, Schweitzer ES, Segal MR, Finkbeiner S (2004). Inclusion body formation reduces levels of mutant huntingtin and the risk of neuronal death. *Nature* 431: 805-810.
2. Atsuta N, Watanabe H, Ito M, Banno H, Suzuki K, Katsuno M, Tanaka F, Tamakoshi A, Sobue G (2006). Natural history of spinal and bulbar muscular atrophy (SBMA): a study of 223 Japanese patients. *Brain* 129: 1446-1455.
3. Banno H, Katsuno M, Suzuki K, Takeuchi Y, Kawashima M, Suga N, Takamori M, Ito M, Nakamura T, Matsuo K, Yamada S, Oki Y, Adachi H, Minamiyama M, Waza M, Atsuta N, Watanabe H, Fujimoto Y, Nakashima T, Tanaka F, Doyu M, Sobue G (2009). Phase 2 trial of leuprorelin in patients with spinal and bulbar muscular atrophy. *Ann Neur* 65: 140-150.
4. Dias FA, Munhoz RP, Raskin S, Werneck LC, Teive HAG (2011). Tremor in X-linked recessive spinal and bulbar muscular atrophy (Kennedy's disease). *Clinics* 66: 955-957.
5. Doyu M, Sobue G, Mukai E, Kachi T, Yasuda T, Mitsuma T, Takahashi A (1992). Severity of X-linked recessive bulbospinal neuronopathy correlates with size of the tandem CAG repeat in androgen receptor gene. *Ann Neurol* 32: 707-710.

6. Fernández-Rhodes LE, Kokkinis AD, White MJ, Watts CA, Auh S, Jeffries NO, Shrader JA, Lehky TJ, Li L, Ryder JE, Levy EW, Solomon BI, Harris-Love MO, La Pean A, Schindler AB, Chen C, Di Prospero NA, Fischbeck KH (2011). Efficacy and safety of dutasteride in patients with spinal and bulbar muscular atrophy: a randomised placebo-controlled trial. *Lancet Neurol* 10: 140-147.
7. Gatchel JR, Zoghbi HY (2005). Diseases of unstable repeat expansion: mechanisms and common principles. *Nat Rev Genet* 10: 743-755.
8. Ishihara H, Kanda F, Nishio H, Sumino K, Chihara K (2001). Clinical features and skewed X-chromosome inactivation in female carriers of X-linked recessive spinal and bulbar muscular atrophy. *J Neurol* 248: 856-860.
9. Katsuno M, Adachi H, Doyu M, Minamiyama M, Sang C, Kobayashi Y, Inukai A, Sobue G (2003). Leuprorelin rescues polyglutamine-dependent phenotypes in a transgenic mouse model of spinal and bulbar muscular atrophy. *Nature Med* 9: 768-773.
10. Katsuno, M., Adachi, H., Kume, A., Li, M., Nakagomi, Y., Niwa, H., Sang, C., Kobayashi, Y., Doyu, M., and Sobue, G. (2002). Testosterone reduction prevents phenotypic expression in a transgenic mouse model of spinal and bulbar muscular atrophy. *Neuron* 35: 843–854.

11. Katsuno M, Adachi H, Minamiyama M, Waza M, Tokui K, Banno H, Suzuki K, Onoda Y, Tanaka F, Doyu M, Sobue G (2006). Reversible disruption of dynactin 1-mediated retrograde axonal transport in polyglutamine-induced motor neuron degeneration. *J Neurosci* 26: 12106-12117.
  
12. Katsuno M, Banno H, Suzuki K, *et al* (2010). Efficacy and safety of leuprorelin in patients with spinal and bulbar muscular atrophy (JASMITT study): a multicentre, randomised, double-blind, placebo-controlled trial. *Lancet Neurol* 9: 875-884.
  
13. Kennedy WR, Alter M, Sung JH (1968). Progressive proximal spinal and bulbar muscular atrophy of late onset: a sex-linked recessive trait. *Neurology* 18: 671-680.
  
14. La Spada AR, Wilson EM, Lubahn DB, Harding AE, Fischbeck KH (1991). Androgen receptor gene mutations in X-linked spinal and bulbar muscular atrophy. *Nature* 352: 77-79.
  
15. La Spada AR, Roling D, Harding AE, Warner CL, Spiegel R, Hausmanowa-Petrusewicz I, Yee WC, Fischbeck KH (1992). Meiotic stability and genotype-phenotype correlation of the trinucleotide repeat in X-linked spinal and bulbar muscular atrophy. *Nature Genet* 2: 301-304.

16. Li M, Miwa S, Kobayashi Y, Merry DE, Tanaka F, Doyu M, Mitsuma T, Hashizume Y, Fischbeck KH, Sobue G (1998). Nuclear inclusions of the androgen receptor protein in spinal and bulbar muscular atrophy. *Ann Neurol* 44: 249-254.
17. Lieberman AP, Harmison G, Strand AD, Olson JM, Fischbeck KH (2002). Altered transcriptional regulation in cells expressing the expanded polyglutamine androgen receptor. *Hum Mol Genet* 11: 1967-1976.
18. McCampbell A, Taylor JP, Taye AA, Robitschek J, Li M, Walcott J, Merry D, Chai Y, Paulson H, Sobue G, Fischbeck KH (2000). CREB-binding protein sequestration by expanded polyglutamine. *Hum Mol Genet* 9: 2197-2202.
19. Miller J, Arrasate M, Brooks E, Libeu CP, Legleiter J, Hatters D, Curtis J, Cheung K, Krishnan P, Mitra S, Widjaja K, Shaby BA, Lotz GP, Newhouse Y, Mitchell EJ, Osmand A, Gray M, Thulasiramin V, Saudou F, Segal M, Yang XW, Masliah E, Thompson LM, Muchowski PJ, Weisgraber KH, Finkbeiner S (2011). Identifying polyglutamine protein species in situ that best predict neurodegeneration. *Nat Chem Biol* 7: 925-934.
20. Minamiyama M, Katsuno M, Adachi H, Waza M, Sang C, Kobayashi Y, Tanaka F, Doyu M, Inukai A, Sobue G (2004). Sodium butyrate ameliorates phenotypic expression in a transgenic mouse model of spinal and bulbar muscular atrophy. *Hum Mol Genet* 13: 1183-1192.

21. Nagashima T, Seko K, Hirose K, Mannen T, Yoshimura S, Arima R, Nagashima K, Morimatsu Y (1988). Familial bulbo-spinal muscular atrophy associated with testicular atrophy and sensory neuropathy (Kennedy-Alter-Sung syndrome). Autopsy case report of two brothers. *J Neurol Sci* 87: 141-152.
  
22. Nedelsky NB, Pennuto M, Smith RB, Palazzolo I, Moore J, Nie Z, Neale G, Taylor JP (2010). Native functions of the androgen receptor are essential to pathogenesis in a *Drosophila* model of spinobulbar muscular atrophy. *Neuron* 67: 936-952.
  
23. Ogata A, Matsuura T, Tashiro K, Moriwaka F, Demura T, Koyanagi T, Nagashima K (1994). Expression of androgen receptor in X-linked spinal and bulbar muscular atrophy and amyotrophic lateral sclerosis. *J Neurol Neurosurg Psychiatry* 57: 1274-1275.
  
24. Preisler N, Andersen G, Thogersen F, Crone C, Jeppesen TD, Wibrand F, Vissing J (2009). Effect of aerobic training in patients with spinal and bulbar muscular atrophy (Kennedy disease). *Neurology* 72: 317-323.
  
25. Ranganathan S, Harmison GG, Meyertholen K, Pennuto M, Burnett BG, Fischbeck KH (2009). Mitochondrial abnormalities in spinal and bulbar muscular atrophy. *Hum Mol Genet* 18: 27-42.

26. Rhodes LE, Freeman BK, Auh S, Kokkinis AD, La Pean A, Chen C, Lehky TJ, Shrader JA, Levy EW, Harris-Love M, Di Prospero NA, Fischbeck KH (2009). Clinical features of spinal and bulbar muscular atrophy. *Brain* 132: 3242-3251.
27. Sinclair R, Greenland KJ, Egmond Sv, Hoedemaker C, Chapman A, Zajac JD (2007). Men with Kennedy disease have a reduced risk of androgenetic alopecia. *Br J Dermatol* 157: 290-294.
28. Sobue G, Matsuoka Y, Mukai E, Takayanagi T, Sobue I (1981). Pathology of myelinated fibers in cervical and lumbar ventral spinal roots in amyotrophic lateral sclerosis. *J Neurol Sci* 50: 413-421.
29. Soraru G, D'Ascenzo C, Polo A, Palmieri A, Baggio L, Vergani L, Gellera C, Moretto G, Pegoraro E, Angelini C (2008). Spinal and bulbar muscular atrophy: skeletal muscle pathology in male patients and heterozygous females. *J Neurol Sci* 264: 100-105.
30. Sumner CJ, Fischbeck KH (2002). Jaw drop in Kennedy's disease. *Neurology* 59: 1471-1472.
31. Yu, Z., Dadgar, N., Albertelli, M., Gruis, K., Jordan, C., Robins, D.M., and Lieberman, A.P. (2006). Androgen-dependent pathology demonstrates

- myopathic contribution to the Kennedy disease phenotype in a mouse knock-in model. *J. Clin. Invest* 116: 2663–2672.
32. Walcott JL, Merry DE (2002). Ligand promotes intranuclear inclusions in a novel cell model of spinal and bulbar muscular atrophy. *J Biol Chem* 277: 50855-50859.
33. Zoghbi HY, Orr HT (2000). Glutamine repeats and neurodegeneration. *Annu Rev Neurosci.* 23: 217-247.

## Figure Legends

Figure 1. Video swallow study in a patient with Kennedy's Disease showing before (a.) and after (b.) swallow with retention of bolus at the base of the tongue and post-cricoid regions. Slow propulsion of liquid in the upper esophagus prior to the aortic arch (c.).

Figure 2. Tongue atrophy in a patient with Kennedy's disease.

**Figures**

Figure 1

**a.**

**b.**

**c.**

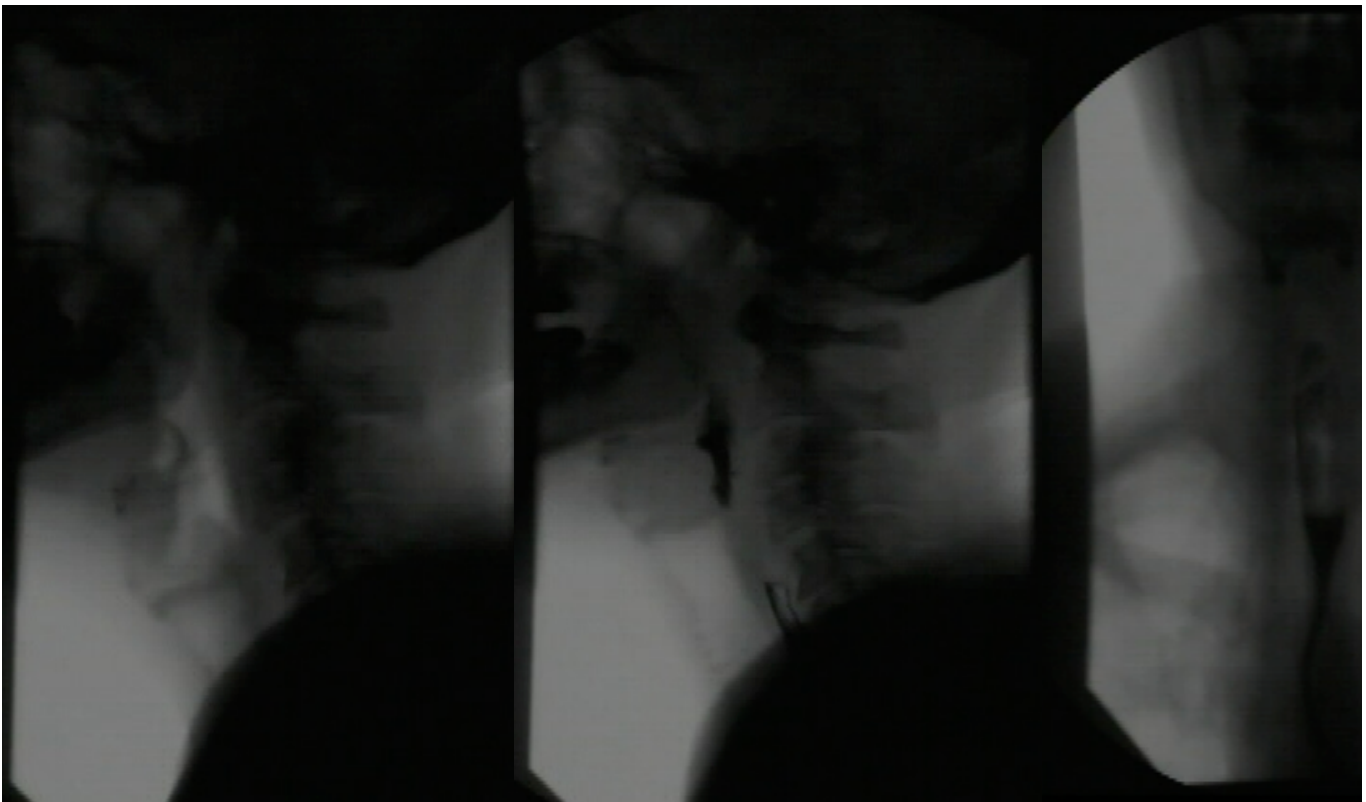
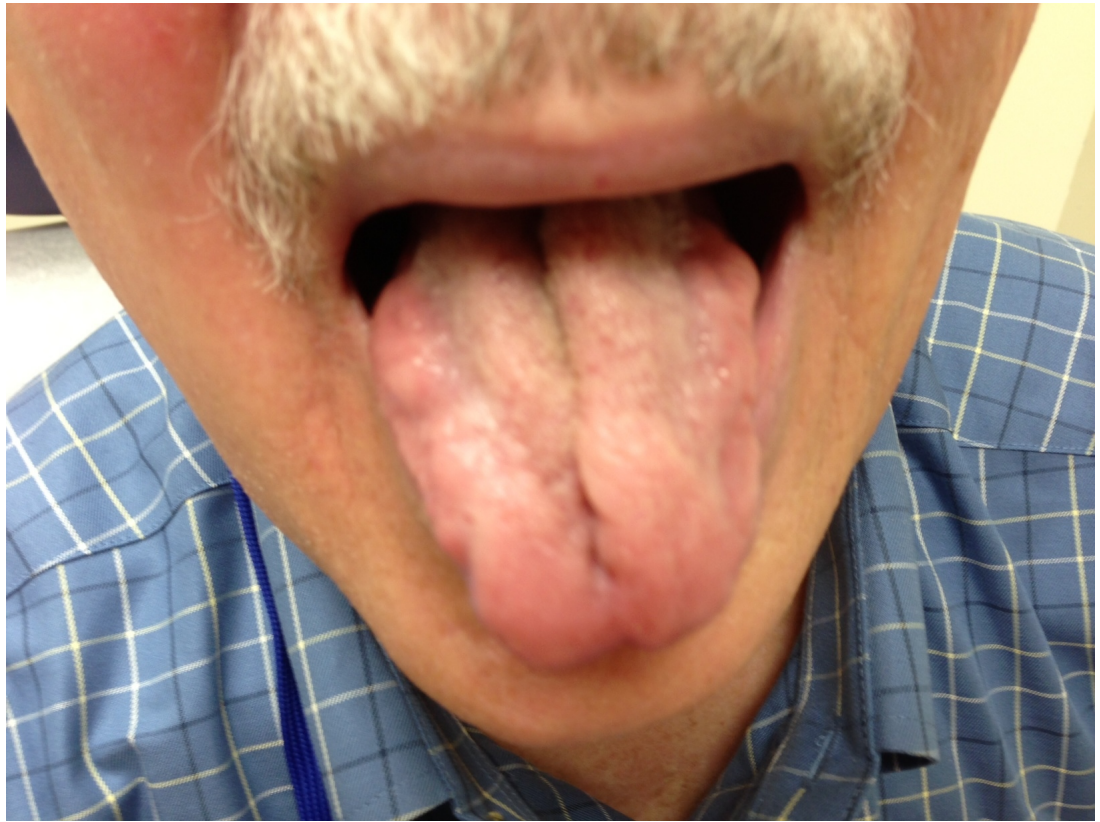


Figure 2



## **Chapter 2-2**

### **Case Report: Early onset and novel features in a spinal-bulbar muscular atrophy patient with a 68 CAG repeat**

**Christopher Grunseich, MD,<sup>1</sup> Ilona R. Kats, BA,<sup>1</sup> Laura C. Bott, MS,<sup>1,2</sup> Carlo Rinaldi,  
MD,<sup>1</sup> Angela Kokkinis, RN,<sup>1</sup> Derrick Fox, MD,<sup>1</sup> Ke-lian Chen, BS,<sup>1</sup> Alice Schindler,  
CGC,<sup>1</sup> Joseph A. Shrader BS PT,<sup>3</sup> Chia-Ying Liu, PhD,<sup>4</sup> Kenneth H. Fischbeck, MD<sup>1</sup>**

Neurogenetics Branch, National Institute of Neurological Disorders and Stroke, NIH,  
Bethesda, MD 20892, USA

Department of Cell and Molecular Biology, Karolinska Institute, 17177 Stockholm,  
Sweden

Rehabilitation Medicine Department, Clinical Center, NIH, Bethesda, MD 20892,  
USA

Radiology and Imaging Sciences, Clinical Center, NIH, Bethesda, MD 20892, US

**Submitted**

**Case.** We report the case of a 29-year-old male who had muscle weakness in his thighs, fatigue after exercise, fasciculations, cramping, and tremor since age 18. He has also had burning neuropathic pain with dysesthesia in the distal lower extremities for the past two years. He occasionally takes ibuprofen to alleviate the pain in his feet. He has no difficulty with swallowing, however, he does experience fatigue in the muscles of mastication after a meal. He will occasionally experience phlegm building up in his throat, although he has not had difficulty with choking. In addition to the neurological features, he had a congenital abnormality of the penis (chordee), which was repaired at age 7. He also has bilateral testicular atrophy. By age 16 he developed gynecomastia, which became socially stigmatizing. He has a pertinent family history of a maternal second cousin with similar neuromuscular symptoms at age 19.

On examination the patient had pronounced gynecomastia bilaterally. Fibrillations and atrophy were noted in the tongue, and weakness was also observed in the orbicularis oculi and orbicularis oris. Limb weakness was severe in the shoulders, thighs, and toes bilaterally. Sensory testing showed a loss of temperature and vibratory sensation in the fingers and toes with a length-dependent gradient. On gait testing he had difficulty standing on his heels or toes. Abnormalities in quantitative muscle strength testing and muscle MRI were also detected (figure, A & B), demonstrating the extent of disease involvement at a relatively early age.

***Detection of a 68 CAG repeat expansion in the androgen receptor.*** Sequencing and PCR analysis of genomic DNA isolated from the patient's venous blood and forearm skin fibroblasts showed a repeat length of 68 CAGs in both samples. Figure C shows a DNA fragment obtained by PCR with primers flanking the CAG repeat run on a 20% acrylamide gel with a DNA fragment obtained from a different patient containing 62 CAGs. Sequencing of the remaining androgen receptor open reading frame of this individual was done and no other genetic variants were found. In particular, the glycine repeat length was in the normal range.<sup>3</sup> Androgen receptor protein levels in patient-derived fibroblasts were comparable to control samples with non-expanded androgen receptor (figure, D).

**Discussion.** Patients with SBMA usually present with the onset of weakness in their mid-forties and have an average androgen receptor repeat length of 47 CAGs.<sup>2</sup> Here we describe a patient with a 68 CAG repeat who has an onset of weakness beginning at age 18 and additional features of disease which have not previously been reported, including abnormalities in sexual development and neuropathic pain. The identification of a patient with 68 CAGs expands the spectrum of disease features associated with SBMA, as the disease has previously been reported in patients with 62 CAGs or less.

The association of a polyglutamine repeat expansion in the androgen receptor with a chordee deformity is novel but not unexpected, given the known expression of androgen receptor in sexually dimorphic tissues. Features of androgen

insensitivity including infertility, gynecomastia, and reduced androgenic alopecia<sup>4</sup> have been described in SBMA. It is possible that the additional findings of chordee and probable small fiber neuropathy observed in this patient are due to the larger expansion of the polyglutamine repeat. Ogata *et al.*<sup>5</sup> reported the identification of a 44 CAG repeat in the androgen receptor of an 11 year old boy with under-masculinized genitalia and chordee without neuromuscular disease. The diagnosis of 5 $\alpha$ -reductase deficiency has also been reported in a pediatric male patient with chordee and normal androgen receptor studies.<sup>6</sup> Treatment of this infant with dihydrotestosterone and surgical release of chordee resulted in improvement of symptoms. Collectively, these findings emphasize that the CAG repeat expansion in the androgen receptor gene is capable of altering androgen-dependent signaling pathways. Our observations further suggest that the CAG expansion mutation may result in damage to pain fibers in the disease.

## References

1. Atsuta N, Watanabe H, Ito M, et al. Natural history of spinal and bulbar muscular atrophy (SBMA): a study of 223 Japanese patients. *Brain* 2006;129:1446-1455.
2. Rhodes LE, Freeman BK, Auh S, et al. Clinical features of spinal and bulbar muscular atrophy. *Brain* 2009;132:3242-3251.
3. Ding D, Xu L, Menon M, et al. Effect of GGC (Glycine) repeat length polymorphism in the human androgen receptor on androgen action. *Prostate* 2005;62:133-139.
4. Sinclair R, Greenland KJ, van Egmond S, et al. Men with Kennedy disease have a reduced risk of androgenetic alopecia. *Br J Dermatol* 2007;157:290-294.
5. Ogata T, Muroya K, Ishii T, et al. Undermasculinized genitalia in a boy with an abnormally expanded CAG repeat length in the androgen receptor gene. *Clin Endocrinol (Oxf)* 2001;53:835-838.

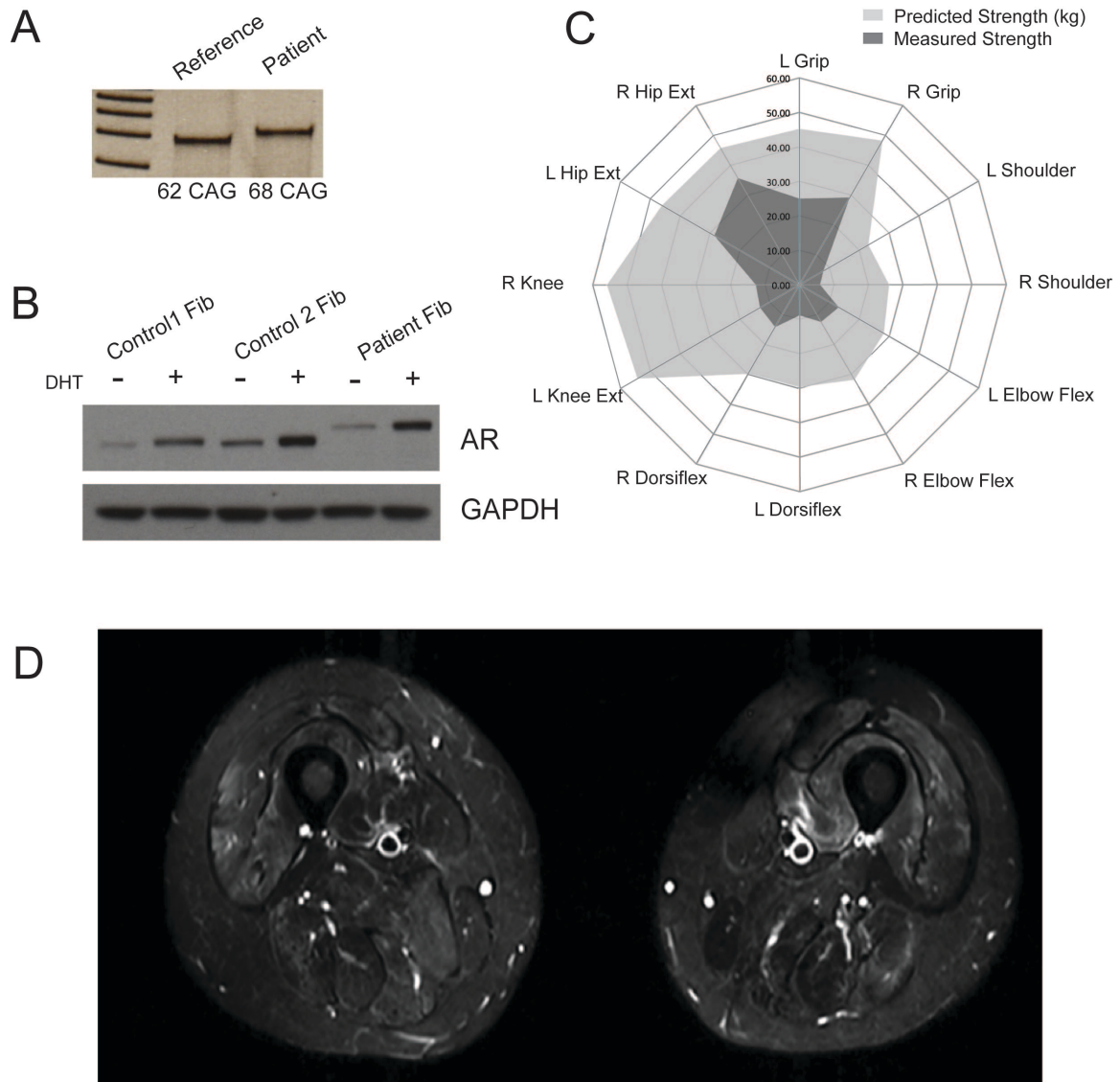
6. Carpenter TO, Imperato-McGinley J, Boulware SD et al. Variable expression of 5 $\alpha$ -reductase deficiency: presentation with male phenotype in a child of greek origin. *J Clin Endocrinol Metab* 1990;71:318-322.

### Figure Legends

#### Figure 1. **Phenotypical features and androgen receptor characterization.**

Quantitative muscle strength testing in 12 different muscle groups shows the degree of muscle weakness (in kg) as compared to controls matched for age, height, weight, and body size (A). T1 STIR MRI image of the thighs showing patchy areas of hyperintensity indicative of muscle injury and degeneration (B). PCR products from patient DNA were generated using primers that bracket the CAG expansion. Acrylamide gel electrophoresis shows the band shift relative to a 62 CAG sample from a different patient (C). Androgen receptor expression is equal in patient derived fibroblast cultures when compared to control samples on western blotting. Dihydrotestosterone (DHT) treatment results in similar upregulation of androgen receptor levels in all samples evaluated (D).

Figure 1



## **Chapter 2-3**

### **IGF-1 ameliorates disease manifestations in a mouse model of SBMA**

**Carlo Rinaldi, MD<sup>1,2</sup> Laura C. Bott,<sup>3,1</sup> Ke-lian Chen,<sup>1</sup> George G. Harmison,<sup>1</sup>**

**Masahisa Katsuno, MD, PhD,<sup>5</sup> Gen Sobue, MD, PhD,<sup>5</sup> Maria Pennuto, PhD,<sup>4</sup>**

**Kenneth H. Fischbeck, MD<sup>1</sup>**

<sup>1</sup> Neurogenetics Branch, National Institute of Neurological Disorders and Stroke (NINDS), NIH, Bethesda 20892, MD, USA.

<sup>2</sup> Department of Neurological Sciences, Federico II University, Naples, 80121, Italy

<sup>3</sup> Department of Cell and Molecular Biology, Karolinska Institutet, Stockholm SE-171 77, Sweden

<sup>4</sup> Department of Neuroscience and Brain Technologies, Istituto Italiano di Tecnologia, Genoa 16163, Italy

<sup>5</sup> Department of Neurology, Graduate School of Medicine, Nagoya University, Nagoya 466-8550, Japan.

## Introduction

Spinal and bulbar muscular atrophy (SBMA, Kennedy's disease) is an X-linked neurodegenerative disorder caused by expansion of a polyglutamine tract in the androgen receptor (AR).<sup>1</sup> The repeat expansion mutation confers a toxic gain of function on the mutant AR protein and results in its aggregation and accumulation into inclusions.<sup>2</sup> The disease is clinically characterized by late-onset weakness and atrophy of extremity and bulbar muscles due to lower motor neuron degeneration in the spinal cord and brainstem; there is also evidence of primary skeletal muscle involvement.<sup>3</sup> Signs of androgen insensitivity are frequently observed.<sup>4</sup> Post-translational modification of the disease protein affects its toxicity.<sup>5,6</sup> We recently showed that insulin-like growth factor 1 (IGF-1) modifies mutant AR toxicity via Akt phosphorylation *in vitro*<sup>7</sup> and that SBMA model mice overexpressing the non-circulating muscle-specific isoform of IGF-1 have a less severe phenotype.<sup>8</sup>

In the present study, we explored the efficacy of parenteral administration of recombinant human IGF-1 and IGF-1 binding protein 3 (rhIGF-1/IGFBP3) in SBMA mice. In order to have clinically meaningful results, we designed the study in a randomized, controlled, blinded fashion, and the treatment was started after the onset of disease manifestations.

## Materials and Methods

*Animals and drug treatment.* The study was carried out in accordance with the NIH Guide for the Care and Use of Laboratory Animals, and was approved by the NINDS Animal Care Committee. Transgenic mice expressing mutant AR with a 97 glutamine repeat (AR97Q) were used.<sup>9</sup> The mice were genotyped by PCR with tail DNA as previously described.<sup>9</sup> Recombinant human IGF-1 in complex with IGFBP-3 (Iplex, mecasemin rinfabate) was provided by Insmad Inc. A vehicle solution was used as control. The injections and all the analyses were performed by blinded investigators.

*Behavioral and survival analysis.* A hanging wire test was performed as previously described.<sup>10</sup> We assessed the gait using the Gait Analysis Treadmill (Columbus Instruments) and TreadScan software (CleverSys). For survival analysis, mice were sacrificed when they had lost more than 30% of body weight, or showed inability to move or signs of dehydration.

*Biochemical analysis.* 16 week old mice were anesthetized with isoflurane and sacrificed. Quadriceps muscles and spinal cord were dissected and snap-frozen in liquid nitrogen. Using a polytron homogenizer, tissue samples were processed in ice-cold homogenization buffer (150 mM NaCl, 50 mM Tris, 2 mM EDTA, 1% sodium deoxycholate, 0.5% Triton X-100, 0.1% sodium dodecyl sulfate) containing protease and phosphatase inhibitor cocktails (Roche). The homogenates were sonicated and pre-cleared at 4,000 x *g* for 10 min at 4°C. Protein lysates were separated on Tris-glycine gels, transferred to PVDF membranes (both Invitrogen), and probed with

the following antibodies: AR H-280 (sc-13062, Santa Cruz), phospho-Akt and total Akt (9271 and 9272, respectively, Cell Signaling), choline acetyltransferase (AB144P, Chemicon), and alpha-tubulin as a loading control (T6199, Sigma). Western blots were visualized with peroxidase-linked secondary antibodies (R&D Systems) by chemiluminescence detection (PerkinElmer Life Sciences). Quantification was done with ImageJ software.

*Histological analysis.* 6-8  $\mu\text{m}$  sections of unfixed, snap frozen quadriceps muscle from 16 week old mice were cut with a  $-20^{\circ}\text{C}$  cryostat and processed for hematoxylin and eosin or nicotinamide adenine dinucleotide staining. For immunofluorescence, sections were fixed with 4% PFA and incubated overnight at  $4^{\circ}\text{C}$  with rabbit anti-laminin (1:80, SIGMA-Aldrich). Digital images were captured using a Zeiss Axiovert 100M microscope and analyzed with NIS Elements software. 8  $\mu\text{m}$  thick tissue sections were fixed in 4% paraformaldehyde, stained with mouse 1C2 antibody (1:20000; Chemicon) and counterstained with Mayer's hematoxylin. For muscle morphology, more than 500 fibers were counted in randomly selected areas. For motor neuron counts, spinal cords from anesthetized mice were collected and post-fixed for 12 h in 4% PFA. Paraffin-embedded samples were serially sectioned at 6  $\mu\text{m}$  steps, mounted on slides, and processed for Nissl staining. Images of ten contiguous sections, 100  $\mu\text{m}$  apart (original magnification, 10 $\times$ ) were analyzed. Motor neurons were identified as cells with Nissl staining, clear nucleus and nucleolus, and a maximum diameter greater than 25  $\mu\text{m}$ .

*Statistical analysis.* A two-way mixed design ANOVA was done to assess the effects of treatment on hanging wire performance and body weight over time. A log rank test was used to compare Kaplan-Meier survival in treated versus non-treated AR97Q mice. A two-tailed Student's t test or, for data not normally distributed, a Mann-Whitney *U* test was performed to compare differences between two groups. The data were analyzed using SPSS version 18 software, and  $p \leq 0.05$  was considered significant.

## Results

*IGF-1 activates Akt and reduces mutant AR aggregation in muscle.* To investigate whether IGF-1 treatment is effective in SBMA mice, we randomized a cohort of male AR97Q mice to receive by daily intraperitoneal injections of either vehicle or rhIGF-1/IGFBP3 (15 mg/kg). This agent mimics the biological effects of IGF-1 alone, but has a more favorable pharmacokinetic profile.<sup>11</sup> We started treatment at age 10 weeks, after the usual onset of disease manifestations.<sup>9</sup> IGF-1 resulted in a significant increase in Akt phosphorylation at serine 473 ( $p < 0.01$ ; Fig 1A) and also reduced the accumulation of both monomeric and aggregated mutant AR ( $p < 0.05$ ,  $p < 0.01$ ; Fig 1B) in skeletal muscle. To assess whether IGF-1 affects the accumulation of mutant AR into nuclear inclusions, cross-sections of quadriceps muscle were stained with the polyglutamine-specific antibody 1C2. IGF-1 reduced the number of 1C2-positive nuclei by about half ( $p = 0.03$ ; Fig 1C).

No changes in the level of Akt phosphorylation (Supplemental Fig 1A) and the accumulation of monomeric and aggregated mutant AR (Supplemental Fig 1B) were detected in spinal cord lysates. To further characterize the effects of IGF-1 on the motor neurons, we analyzed spinal cord levels of choline acetyltransferase (ChAT), a cholinergic neuron marker. ChAT levels were higher in IGF-1 treated mice than in vehicle-treated animals ( $p = 0.01$ ; Supplementary Fig 1C) and comparable to wild type littermates (not shown).

*IGF-1 administration attenuates disease manifestations in SBMA mice.* Forty male transgenic mice were randomly assigned to receive either vehicle or IGF-1 from 10 through 20 weeks of age, as described above. IGF-1 treated SBMA mice had less body weight loss ( $p = 0.001$ ; Fig 2A and B) and increased grip strength ( $p = 0.001$ ; Fig 2C). Gait analysis at week 16, showed longer stride time and length and reduced rear track width and paw area in the IGF-1 treated SBMA mice (Fig 2D). Mice treated with IGF-1 lived ~3 weeks longer on average than vehicle-treated mice, although this did not reach statistical significance ( $p = 0.09$ ; Fig 2E), in part because a subset of the mice were already severely affected before the beginning of treatment. A post hoc analysis excluding these mice (hunched posture and sustained weight loss > 5% at week 10) showed a significant difference between the remaining animals in the two groups ( $p = 0.02$ ; Supplemental Fig 1D).

*IGF-1 reduces muscle pathology in AR97Q mice.* To investigate the effects of IGF-1 treatment on muscle pathology, quadriceps muscles were collected from 16

week old SBMA mice and wild type littermates treated with vehicle or IGF-1. Muscle cross-sections of vehicle-treated AR97Q mice showed angulated myofibers and grouped atrophic fibers, as well as fibers with central nuclei (Fig 3A-B). These signs of muscle atrophy and degeneration were markedly reduced in the IGF-1-treated mice. The mean cross-sectional area and minimal diameter of myofibers were also increased compared to vehicle-treated mice ( $p = 0.01, 0.03$ , respectively; Fig 3C-E). There was a slight increase in the number of anterior horn cells in mice treated with IGF-1, but it did not reach statistical significance ( $p = 0.09$ ; Supplementary Fig 1E). This is not surprising since the motor neuron count is not significantly reduced in this mouse model.<sup>9</sup>

## Discussion

In this study, we evaluated the effects of parenteral administration of IGF-1 in a mouse model of SBMA. IGF-1 improved motor performance, attenuated weight loss, and improved muscle pathology in SBMA mice. It also had indirect effects on motor neurons, as suggested by the increase in ChAT expression in IGF-1-treated mice. Peripheral delivery of IGF-1 results in very low concentrations in brain, but skeletal muscle is a source of signals that influence motor neuron maintenance.<sup>12</sup>

IGF-1 and other trophic factors have been evaluated as potential treatments for amyotrophic lateral sclerosis, due to their effects on promoting muscle growth<sup>13</sup>

and motor neuron survival.<sup>14</sup> However, the response of this disease to IGF-1 therapy has been not beneficial to date.<sup>15,16,17</sup>

SBMA may be a better candidate for IGF-1 administration for two reasons: 1) IGF-1, via Akt phosphorylation, specifically reduces the toxicity of mutant AR;<sup>7,8</sup> and 2) muscle has a role in the pathogenesis of SBMA. Muscle biopsies from SBMA patients show myogenic changes as well as neurogenic atrophy;<sup>18</sup> muscle pathology precedes spinal cord pathology in a knockin mouse model of SBMA;<sup>19</sup> and muscle-specific overexpression of wild type AR leads to an SBMA-like phenotype.<sup>20</sup>

Our study indicates that peripheral delivery of IGF-1 in SBMA mice has benefit after the onset of disease manifestations. These results provide a pre-clinical basis for further examining IGF-1 in SBMA patients.

### **Acknowledgments**

This work was supported by NINDS intramural research funds. We thank Hiroaki Adachi for helping with the 1C2 immunostaining, Sweta Girgenrath for discussion about dose selection, and Nico P. Dantuma for support. Laura C. Bott was part of the NIH-Karolinska Graduate Partnership Program in Neuroscience. Insmad Inc. kindly provided the study agent and vehicle. Maria Pennuto is supported by grants from Telethon-Italy (GGP10037), the Kennedy's Disease Association, and the Muscular Dystrophy Association (196646).

## References

1. La Spada AR, Wilson EM, Lubahn DB, et al. Androgen receptor gene mutations in X-linked spinal and bulbar muscular atrophy. *Nature* 1991;352:77–79.
2. Adachi H, Katsuno M, Minamiyama M, et al. Widespread nuclear and cytoplasmic accumulation of mutant androgen receptor in SBMA patients. *Brain* 2005;128:659-670.
3. Katsuno M, Adachi H, Waza M, et al. Pathogenesis, animal models and therapeutics in spinal and bulbar muscular atrophy (SBMA). *Exp Neurol* 2006;200:8–18.
4. Sinnreich M, Klein CJ. Bulbospinal muscular atrophy: Kennedy's disease. *Arch Neurol* 2004;61:1324-1326.
5. Emamian ES, Kaytor MD, Duwick LA, et al. Serine 776 of ataxin-1 is critical for polyglutamine-induced disease in SCA1 transgenic mice. *Neuron* 2003;38:375-387.

6. Gu X, Greiner ER, Mishra R, et al. Serines 13 and 16 are critical determinants of full-length human mutant huntingtin induced disease pathogenesis in HD mice. *Neuron* 2009;64:828-840.
  
7. Palazzolo I, Burnett BG, Young JE, et al. Akt blocks ligand binding and protects against expanded polyglutamine androgen receptor toxicity. *Hum Mol Genet* 2007;16:1593–1603.
  
8. Palazzolo I, Stack C, Kong L, et al. Overexpression of IGF-1 in muscle attenuates disease in a mouse model of spinal and bulbar muscular atrophy. *Neuron* 2009;63:316-328.
  
9. Katsuno M, Adachi H, Kume A, et al. Testosterone reduction prevents phenotypic expression in a transgenic mouse model of spinal bulbar muscular atrophy. *Neuron* 2002;35:843-854.
  
10. Crawley JN. *What's wrong with my mouse?* Hoboken, NJ: John Wiley & Sons. Inc., 2007.

11. Camacho-Hübner C, Rose S, Preece MA, et al. Pharmacokinetic studies of recombinant human insulin-like growth factor 1 (rhIGF-1)/rhIGF-binding protine-3 complex administered to patients with growth hormone insensitivity syndrome. *J Clin Endocrinol Metab* 2006;91:1246-1253.
  
12. Funakoshi H, Belluardo N, Arenas E, et al. Muscle-derived neurotrophin-4 as an activity-dependent trophic signal for adult motor neurons. *Science* 1995;268:1495-1499
  
13. Sandri M, Sandri C, Gilbert A, et al. Foxo transcription factors induce the atrophy-related ubiquitin ligase atrogen-1 and cause skeletal muscle atrophy. *Cell* 2004;117:399-412.
  
14. Caroni P, Grandes P. Nerve sprouting in innervated adult skeletal muscle induced to exposure to elevated levels of insulin-like growth factors. *J Cell Biol* 1990;110:1307-1317.

15. Lai EC, Felice KJ, Festoff BW, et al. Effect of recombinant human insulin-like growth factor-I on progression of ALS. A placebo-controlled study. The North America ALS/IGF-I Study Group. *Neurology* 1997;49:1621-1630.
16. Borasio GD, Robberecht W, Leigh PN, et al. A placebo-controlled trial of insulin-like growth factor-I in amyotrophic lateral sclerosis. European ALS/IGF-I Study Group. *Neurology* 1998;51:583-586.
17. Sorenson EJ, Windbank AJ, Mandrekar JN, et al. Subcutaneous IGF-1 is not beneficial in 2-year ALS trial. *Neurology* 2008;71:1770-1775.
18. Sorarù G, D'Ascenzo C, Polo A, et al. Spinal and bulbar muscular atrophy: skeletal muscle pathology in male patients and heterozygous females. *J Neurol Sci* 2008;264:100–105.
19. Yu Z, Dadgar N, Albertelli M, et al. Androgen-dependent pathology demonstrates myopathic contribution to the Kennedy disease phenotype in a mouse knock-in model. *J Clin Invest* 2006;116:2663–2672.
20. Monks DA, Johansen JA, Mo K, et al. Overexpression of wild-type androgen

receptor in muscle recapitulates polyglutamine disease. Proc Natl Acad Sci USA 2007;104:18259–18264.

### Figure Legends

**Figure 1.** IGF-1 increases phosphorylation of Akt and decreases AR aggregation in SBMA muscle. **(A)** Western blot analysis of Akt *phosphorylation* in skeletal muscle. Quantification of Akt, showing the mean with standard deviation. Unpaired t-test \*\*  $p < 0.01$  ( $n = 5$ ). **(B)** Western blot analysis of AR protein levels in skeletal muscle. Quantification, showing the mean with standard deviation. Unpaired t-test, \*  $p < 0.05$ ; \*\*  $p < 0.01$  ( $n = 5$ ). **(C)** Immunohistochemical analysis using 1C2 antibody on cross sections of AR97Q muscle shows a reduction of diffuse nuclear staining and nuclear inclusions in IGF-1 compared to vehicle-treated mice. Graphs, mean  $\pm$  SEM; \*  $p = 0.03$ . Scale bar, 20  $\mu\text{m}$ .

**Figure 2.** IGF-1 attenuates weight loss, enhances motor behavior, and increases survival of SBMA mice. **(A)** Two mice from the same litter at week 16 of age, showing the gross appearance of an IGF-1 treated (left) and vehicle-treated (right) SBMA mouse. **(B and C)** IGF-1 treated SBMA ( $n = 20$ ) mice had less body weight loss ( $p = 0.001$ ) and increased grip strength ( $p = 0.001$ ) compared to vehicle-treated mice ( $n = 20$ ). Scale bars, SEM. **(D)** TreadScan assessment showed improved motor

performance in AR97Q mice treated with IGF-1 (n = 6) compared to vehicle (n = 6). Scale bars, SEM. Unpaired t-test \*\* p < 0.01; \* p < 0.05 (E) Kaplan-Meier survival curves of mice treated with IGF-1 (n = 20) or vehicle (n = 20). P = 0.09, log-rank test.

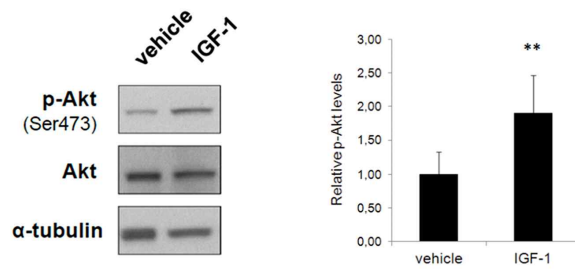
**Figure 3.** IGF-1 ameliorates SBMA muscle pathology. (A) Hematoxylin and eosin staining. Arrows = fibers with central nuclei; asterisks = angulated and grouped fibers. (B) Nicotinamide adenine dinucleotide staining. Asterisks = moth-eaten fibers. (C) Histograms of myofiber cross-sectional area (CSA). (D) Muscle cross-sectional area (CSA) and (E) minimal Feret's diameter were increased in SBMA mice treated with IGF-1 compared with vehicle (p = 0.01 and p = 0.03, respectively). Shown are transverse sections of quadriceps of 16-week-old SBMA mice and wild-type littermates.

**Supplementary Figure 1.** IGF-1 effects on spinal cord pathology in SBMA Mice. (A) Western blot of Akt phosphorylation in spinal cord. Quantification of Akt, showing the mean with standard deviation. Unpaired t-test, p = 1.00. (B) Western blot of AR protein levels in spinal cord of AR97Q mice. Quantification for mutant AR and of the AR aggregates, showing the mean with standard deviation. Unpaired t-test, p = 0.18 and p = 0.13, respectively. (C) Western blot of ChAT levels in spinal cord. Quantification of ChAT level, showing the mean with standard deviation. Unpaired t-test, \* p = 0.01. (D) Kaplan-Meier survival curves of mice treated with IGF-1 (n = 16) or vehicle (n = 18) receiving at least 5 weeks of treatment. P = 0.02, log-rank test. (E) Nissl-stained transverse sections of ventral spinal cords of 16-week-old

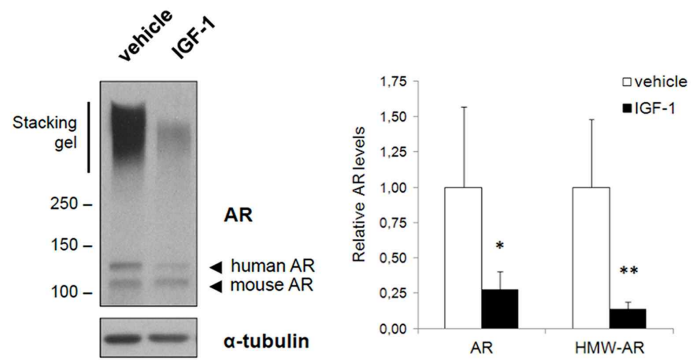
mice. Quantitative analysis suggested an increase in the number of motor neurons per section is slightly increased in AR97Q mice treated with IGF-1 as compared to vehicle, but this did not reach statistical significance ( $p = 0.09$ ). Graphs, mean  $\pm$  SEM,  $n = 3$ .

Figure 1

A



B



C

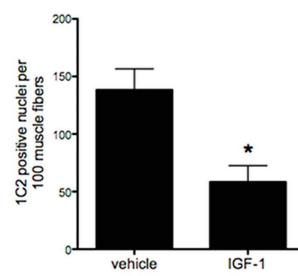
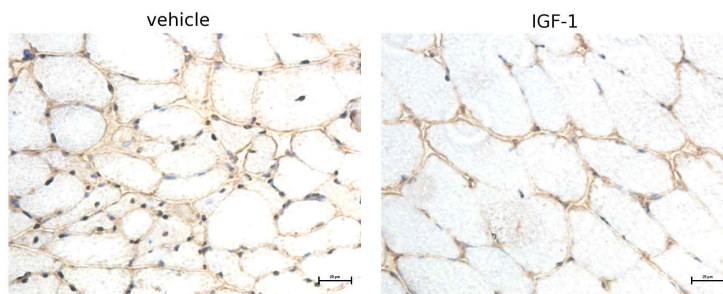


Figure 2

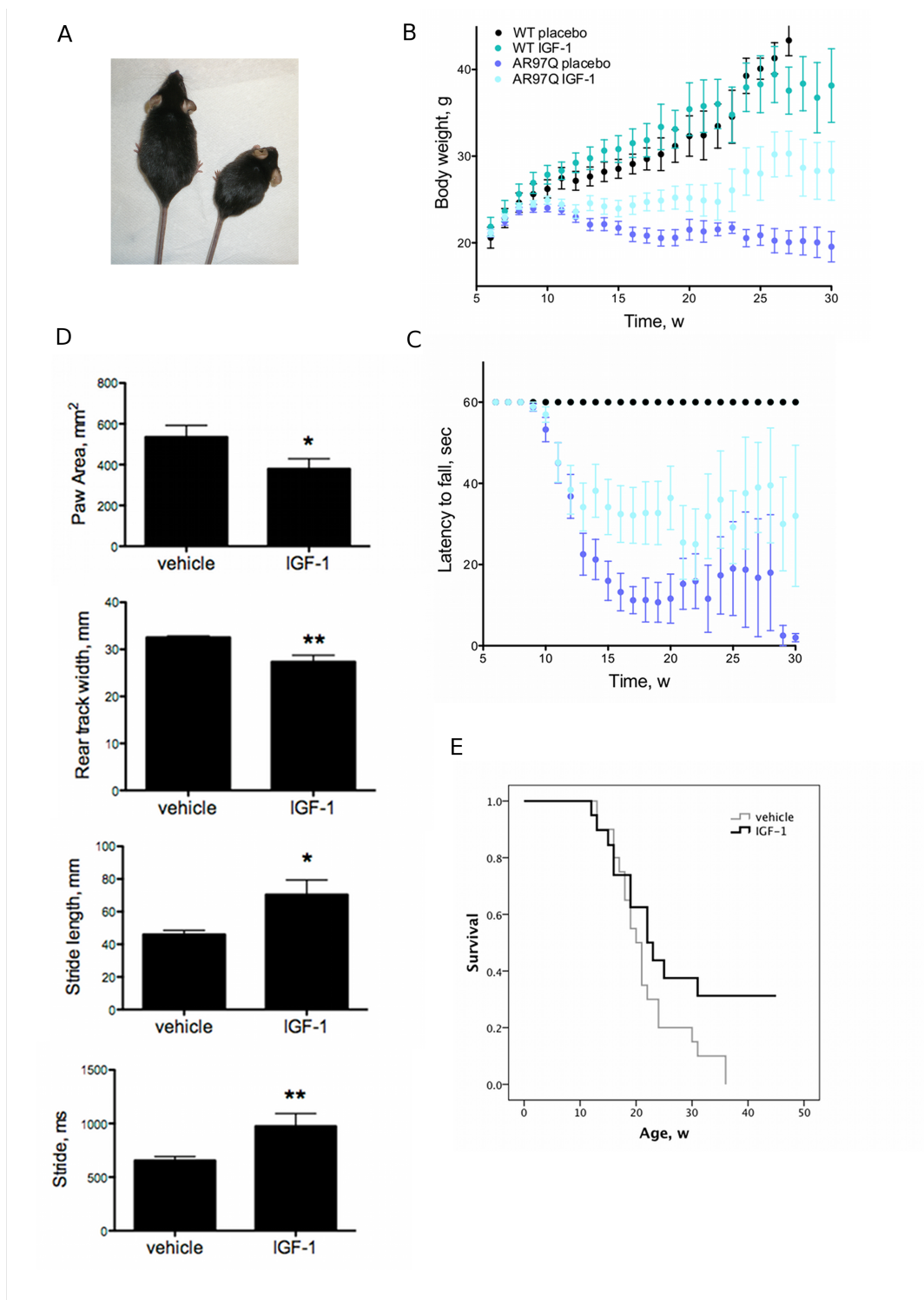
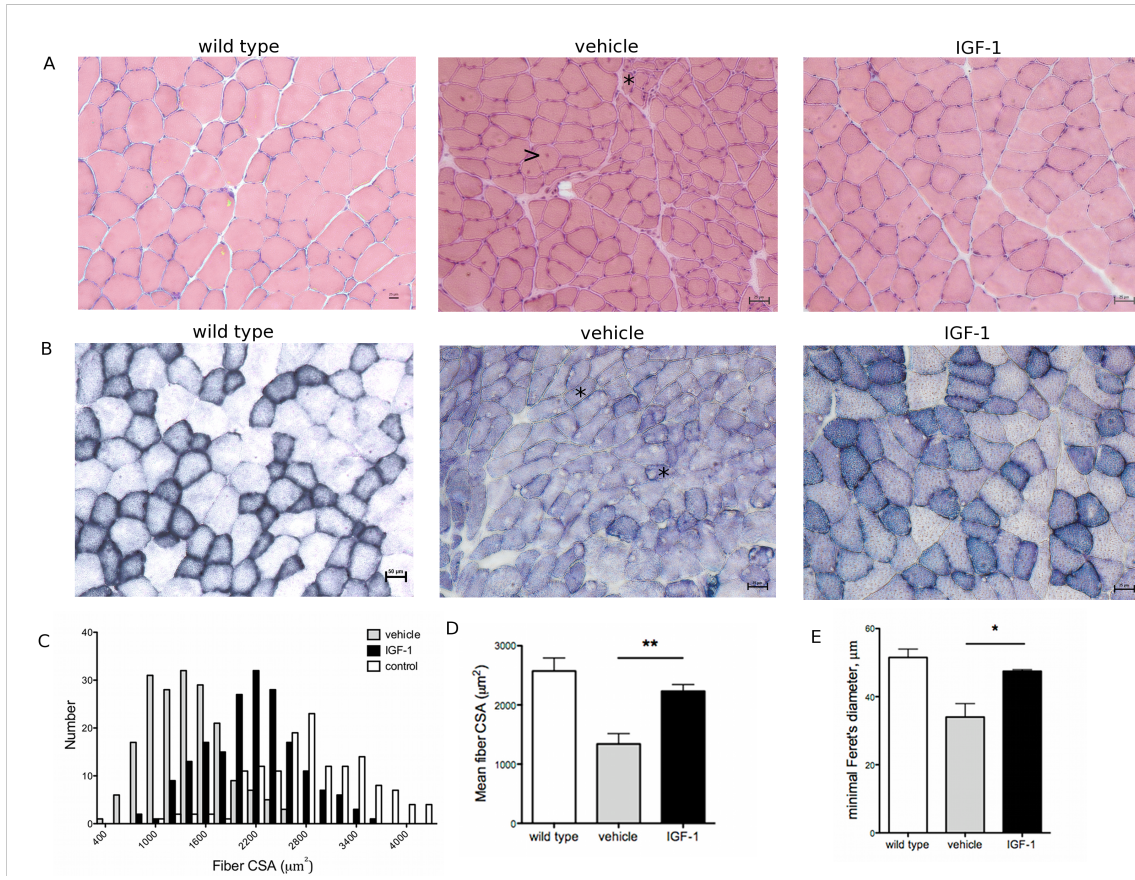
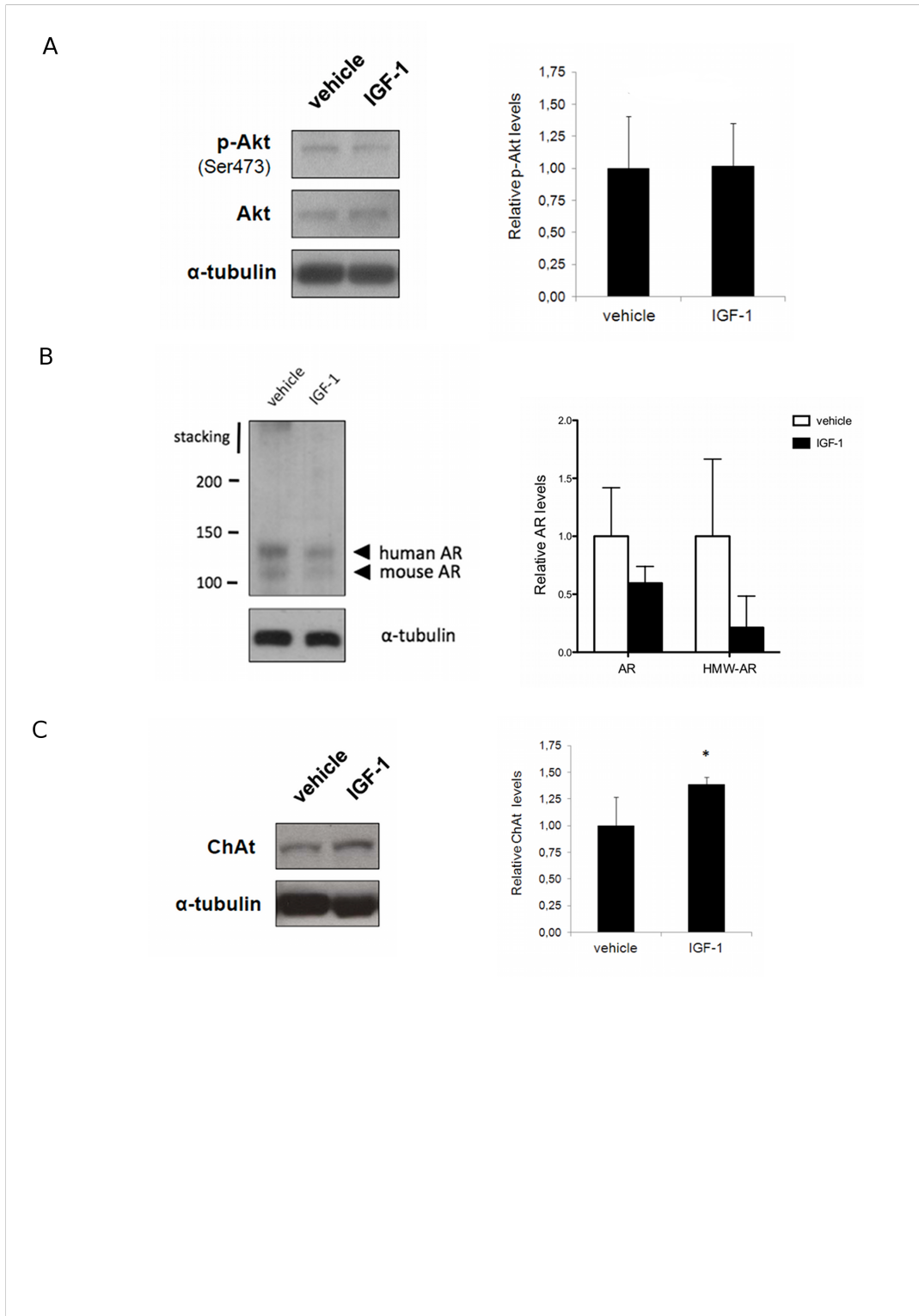


Figure 3



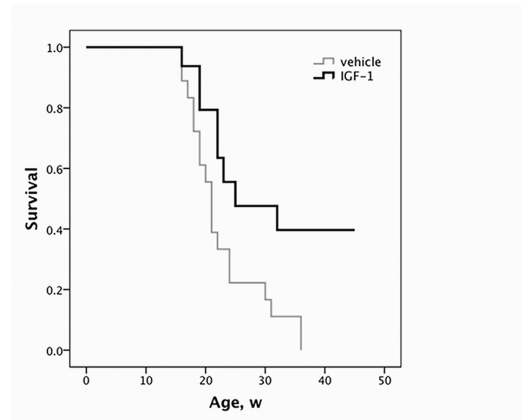
## Supplemental Data



**Supplementary Figure 1.** IGF-1 effects on spinal cord pathology in SBMA Mice.

(A) Western blot of Akt phosphorylation in spinal cord. Quantification of Akt, showing the mean with standard deviation. Unpaired t-test,  $p = 1.00$ . (B) Western blot of AR protein levels in spinal cord of AR97Q mice. Quantification for mutant AR and of the AR aggregates, showing the mean with standard deviation. Unpaired t-test,  $p = 0.18$  and  $p = 0.13$ , respectively. (C) Western blot of ChAT levels in spinal cord. Quantification of ChAT level, showing the mean with standard deviation. Unpaired t-test, \*  $p = 0.01$ . (D) Kaplan-Meier survival curves of mice treated with IGF-1 ( $n = 16$ ) or vehicle ( $n = 18$ ) receiving at least 5 weeks of treatment.  $P = 0.02$ , log-rank test. (E) Nissl-stained transverse sections of ventral spinal cords of 16-week-old mice. Quantitative analysis suggested an increase in the number of motor neurons per section is slightly increased in AR97Q mice treated with IGF-1 as compared to vehicle, but this did not reach statistical significance ( $p = 0.09$ ). Graphs, mean  $\pm$  SEM,  $n = 3$ .

D



E

